Insight into the exchange coupling between magnetic molecules and the supporting surface: spectromicroscopy correlation including X-ray magnetic circular dichroism

Inauguraldissertation

zur

Erlangung der Würde eines Doktors der Philosophie

vorgelegt der

Philosophisch–Naturwissenschaftlichen Fakultät

der Universität Basel

von

Dorota J. Chylarecka

aus Piła (Polen)

Villigen, 2011

Genehmigt von der Philosophisch-Naturwissenschaftlichen Fakultät auf Antrag von:

Prof. Dr. Thomas Jung

Prof. Dr. Ernst Meyer

Basel, den 21 Juni 2011

Prof. Dr. Martin Spiess

Dekan

Abstract

This thesis reports on magnetic properties of organic molecules deposited on ferromagnetic surfaces. Complementary surface science techniques like: scanning tunneling microscopy (STM), X-ray photoelectron spectroscopy (XPS) or low-energy electron diffraction (LEED) have been employed to study the chemical, electronic and structural properties of the interfaces. X-ray magnetic circular dichroism (XMCD), performed at the synchrotron, has given us insights into magnetic interaction of paramagnetic molecules with ferromagnetic substrates. The interpretation of the experimental data has been supported by density functional theory calculations (DFT) performed by a collaborating group of Peter Oppeneer from Uppsala University, Sweden.

The manganese tetraphenyl porphyrin chloride (MnTPPCl) molecules are shown to couple magnetically to the supporting cobalt (Co) thin film. The ordering of the molecular spins is parallel with the spin of the substrate, i.e. it is ferromagnetic. It has been experimentally verified that the coupling originates from an indirect exchange interaction between Mn and Co atoms which is mediated by nitrogen atoms present in the molecular macrocycle. MnTPPCl molecules undergo a partial dissociation on the Co surface, leading to the removal of the chlorine (Cl) ligand and to consequent reduction of the Mn ion oxidation state from 3+ to 2+. Both molecular species have been identified in the STM images. Our results also show that Mn in the MnTPP molecule (after dissociation of the Cl) resides in an intermediate spin configuration.

Modification of the substrate by controlled oxygen exposure and the consequent formation of oxide ad-layer, reduces the molecule-substrate interaction, as evidenced by the emergence of molecular self-assembly, which was not present on the atomically clean Co. Also the MnTPPCl molecule itself now remained intact upon deposition onto the O/Co substrate. Notably, the magnetic interaction on an oxidized surface has transferred into

a superexchange antiferromagnetic coupling, leading to an antiparallel alignment of the Mn and Co spins.

The last experiment presented in this thesis demonstrates the possibility of magnetic switching of a molecular monolayer. We have been able to switch off the magnetisation of MnTPPCl molecules on the surface by supplying nitric oxide (NO) gas as a reactant. NO binds to the Mn in a linear geometry, in which it is formally considered as a three-electron-donor. It could therefore compensate the Mn ion's spin of 3/2 and quench the initially observed XMCD signal. The Mn-NO bond has been shown to resist the thermal treatment and it has not been possible to restore the magnetization of Mn.

Our results have shown that the spectromicroscopy correlation approach, here involving STM, XPS and XMCD, is a powerful tool for the identification of the mechanisms involved in magnetic and structural ordering of the organometallic layers. The combination of such experiments with ab-initio theoretical calculations allows for a detailed description of magnetic processes occurring at the metal-organic interfaces.

Contents

List of abbreviations

The following table is an alphabetical list of abbreviations used throughout the thesis:

AFM	antiferromagnetic
CFT	Crystal Field Theory
DFT	Density Functional Theory
DOS	Density of States
e-beam	electron beam
ESCA	Electron Spectroscopy for Chemical Analysis (old name for XPS)
fcc	face centered cubic
FM	ferromagnetic
GMR	Giant MagnetoResistance
HS	High-Spin
IS	Intermediate-Spin
L	langmuir
LCAO	Linear Combination of Atomic Orbitals
LEED	Low-Energy Electron Diffraction
LFT	Ligand Field Theory
LMN	Laboratory for Micro- and Nanotechnology
LS	Low-Spin
ML	monolayer
MO	Molecular Orbital
MnP	manganese(II) porphyrin
MnTPPCl	manganese(III) tetraphenylporphyrin chloride

NjL	Nanojunction Laboratory
NO	nitric oxide
Pc	phthalocyanine
PSI	Paul Scherrer Institut
QCMB	Quartz Crystal MicroBalance
SEM	Scanning Electron Microscopy/Microscope
SIM	Surfaces/Interfaces: Microscopy
SMM	Single-Molecule Magnet
SLS	Swiss Light Source
SP-STM	Spin-Polarized STM
STM	Scanning Tunneling Microscopy/Microscope
TCNQ	tetracyano-p-quinodimethane
TEY	Total Electron Yield
TPP	tetraphenylporphyrin
UHV	Ultra-High Vacuum
UV-Vis	Ultraviolet-Visible
XAS	X-ray Absorption Spectroscopy
XMCD	X-ray Magnetic Circular Dichroism
XPS	X-ray Photoelectron Spectroscopy

CHAPTER 1

Introduction

Magnetic properties of naturally occurring minerals have been utilized for centuries, but at the beginning little was known about the origin of magnetism. Apart from being used as compass needles for navigation, there were other, quite surprising, applications of magnets:

> "Placed on the pillow of a guilty wife, it would make her confess her iniquities as she slept. It could be used for the treatment of many ailments, and as a contraceptive." [1]

This text from the thirteenth century illustrates, that magnetic properties used to be ascribed to some magical powers, which could also yield such mysterious features. Only in the twentieth century scientists discovered that the magnetism stems from unpaired electrons and their interactions in matter. Although, nowadays magnetic properties of many materials have been measured, described and successfully utilized, still, various magnetic systems pose new and difficult questions.

During the last decades, magnetism in research and technology has evolved from bulk materials to the development of giant magnetoresistance (GMR) and surface/interface magnetism. It is expected [2, 3], that the emerging functional spintronic materials will make decisive use of the interface properties of e.g. the organic/inorganic interfaces.

This thesis reveals new aspects about the magnetic exchange coupling between manganese-porphyrin molecules and cobalt as a ferromagnetic substrate. Interestingly, porphyrins, similarly to the first magnet – lodestone (magnetite), are naturally occurring

materials, which show yet not fully understood magnetic properties. The magnetic coupling described here, is a complex process resulting from various chemical and physical interactions on the surface. Only the combination of spectroscopy and microscopy approaches with density functional theory calculations provide insight into the detailed mechanisms towards a sound understanding and a precise description of the substrate-induced magnetic ordering of organometallic molecules.

Organometallic molecules consist of a transition metal atom surrounded by an organic macrocycle. Interaction of the metal with the ligand field imposed by the macrocycle causes splitting of the valence energy levels of the metal and allows for high-spin configurations [4], which are of great interest due to their magnetic properties. Additionally, the extensively studied organic molecules belong to a family of naturally occurring porphyrins, which makes them an interesting and versatile scientific topic. A prominent example for an organometallic molecule the haem (iron-porphyrin). It is a building block of the haemoglobin protein responsible for the oxygen transport in a human body. Due to the presence of delocalized electrons in the macrocycle and the electron configuration of the iron ion, the haem molecule absorbs green light and as a consequence appears red. The iron ion contains unpaired electrons, is therefore paramagnetic and might be a suitable candidate for spintronic applications.

Spin (dependent elec)tronics (also called magnetoelectronics) is a field of electronics, where electron spin is used to carry information. As a research field, spintronics emerged after the discovery of GMR [5, 6]. Spintronic devices, like the GMR head in current hard disc drive technology, have become the industry standard in the meantime. Usually, ferromagnetic alloys are used in the magnetoelectronic media, but it is foreseen that they might be replaced or complemented by *organic* layers or single molecules [7] in the future. The advantages of organic spintronics include increased data storage densities and reduced device dimensions. Additionally, information stored in an organic-spintronic device should survive longer, as the spin-relaxation times are: $10^{-7} - 10^{-5}$ s compared to 10^{-10} s in metals [8]. Due to the power of chemistry, the properties of organic spintronic materials and interfaces can be tuned by a chemical modification of the base materials and surfaces/interfaces.

Spintronics is dependent on materials containing unpaired spin: either the here studied, *magnetic molecules* or *single molecule magnets* (SMMs) provide interesting alternatives with partially different characteristics. SMMs are paramagnetic molecules which have a single-domain magnetic core exhibiting the magnetization hysteresis below a certain blocking temperature (T_B between sub-Kelvin and $\sim$100 K) when subjected to high (1-4 Tesla) external magnetic fields. They usually contain high spin states of pure molecular origin (not related to any cooperative effect) and are characterized by a bistable magnetic anisotropy generating an energy barrier for the magnetization reversal [9]. Switching of these spin states can occur through magnetic quantum tunneling, or

classically by thermal excitation. The hysteresis loop of an SMM shows characteristic steps which are attributed to the macroscopic manifestation of the field-tuned resonant spin-dependent tunneling [10]. For a long time magnetism of SMMs was shown to vanish when adsorbed as a monolayer on metallic substrates [11, 12]. In 2009 however, Mannini *et al.* showed a monolayer of an SMM on gold retaining its magnetic behaviour at 0.5 K [13].

Magnetic (organometallic) *molecules*, on the other side, were shown to order magnetically in a (sub)monolayer regime on ferromagnetic substrates at room temperature [14]. Like SMMs, they are paramagnetic in their bulk form. As single molecules or layers they show measurable magnetic moments either when magnetically coupled to the substrate or when subjected to high magnetic fields (and sometimes, low temperatures). In 2005 Scheybal *et al.* [14] provided first evidence for the magnetic coupling between a monolayer of organic molecules and a ferromagnetic substrate at room temperature and in remanent magnetic field of the substrate. Scheybal's work was followed up later by Wende *et al.* [15] who explained the nature of the magnetic coupling by means of density functional theory (DFT) calculations. In the past three years a whole avalanche of articles was set off. Iacovita *et al.* [16], for example, showed that the magnetic coupling of a molecule can also be studied by means of spin-polarized scanning tunneling microscopy and spectroscopy (SP-STM and STS). These three articles provided milestones in the development of the scientific understanding of magnetic molecular layers in their coupling to magnetic surfaces, which is the topic of this thesis.

Currently, the scientific knowledge in the field of magnetic molecules and their coupling at surfaces/interfaces is progressing rapidly. Allured by the new opportunities in material science and the potential applications in organic spintronic devices [17–21] many research groups have now entered the field of organic spintronics. Typical for any emerging discipline, the increased competition together with the scientific discussion and verification of earlier results by a growing community of interested scientists and technologists leads to accelerated progress. In order to investigate magnetic, electronic and spintronic properties of well defined interfaces and structures, several complementary techniques are combined in this thesis, in particular surface- and element-specific spectroscopy, tunneling microscopy and numerical simulations.

Before the start of this research project, two molecules were shown to undergo exchange coupling with a magnetic substrate: Mn-porphyrin [14] and Fe-porphyrin [15]. The former molecule has been extensively studied by our group. On the basis of the first study, the magnetic coupling was unambiguously observed, but its origin was not yet understood. Also it remained unclear at that time, whether the molecule stayed intact on the magnetic surface. This provided the starting point for this thesis: (i) repeat the successful measurement from year 2005, (ii) identify the chemical species present on the surface and (iii) explain the origin of the magnetic coupling to the substrate.

We succeeded in achieving all of these goals and also managed to further explore the properties of Mn-porphyrin, amongst some other magnetic molecules which were studied as a reference material. X-ray absorption (XA) and X-ray magnetic circular dichroism (XMCD) experiments are combined with scanning tunneling microscopy (STM), X-ray photoelectron spectroscopy (XPS) and low-energy electron diffraction (LEED) to reveal the details of the molecule-substrate interaction and its influence on the magnetic coupling. Notably, due to a multichamber experimental system and due to the possibility of a vacuum transfer between the main sample preparation and characterization system and the experimental beamline at the synchrotron, all these experiments were possible to be performed on the *same* sample. Complementary numerical calculations were carried out by the group of P. Oppeneer towards the conclusive analysis of the physical processes involved in the magnetic interactions. As we will see in the following chapters, the experimental data do not always agree with the calculations. All experiments presented in this thesis are reproducible and provide confirming results with reasonable error margins related to the expected variability of the sample preparation and detection methods. Simplifications of the numerical models which are needed to reduce the computational time to a reasonable amount, are therefore suspected as the dominant source of the observed differences between experiment and theory. There are many physical and chemical factors which affect the structure and the properties of the magnetic interfaces and they can all be assessed by the here presented spectromicroscopy correlation approach. Therefore, in case of discrepancies between the theory and experiment in this thesis, the experimental results will be credited, as they approach more closely the real system under study.

The knowledge gained by experiments presented here, contributed to a selection of publications about the interaction and the magnetic coupling of organometallic molecules with ferromagnetic substrates. To locate our research within the broad landscape of scientific contributions I will first describe, in the following paragraphs, current advances in the field.

The first follow-up of the seminal work by Scheybal *et al.* reports about detecting a magnetic moment in an iron(III) octaethylporphyrin chloride (FeOEPCl) adsorbed on cobalt (Co) and on nickel (Ni) thin films [15]. In analogy to the initial report, the molecular magnetization is parallel to the magnetization of the substrate in all stages of a hysteresis loop, i.e. it is ferromagnetically aligned to the substrate. This relationship moreover, is confirmed in both magnetization directions of the substrate: in-plane (on Co) as described by Scheybal and also out-of-plane (on Ni). Complementary numerical calculations based on DFT revealed that the Fe(III)OEPCl species cannot couple ferromagnetically to the substrate; instead, antiferromagnetic contributions are expected. Therefore, the simulation of the ferromagnetic coupling was performed for Fe(II)OEP – an analogue of the original molecule lacking the chlorine ligand. This choice

was justified by the observation of Fe XAS peak at the energy position corresponding to a 2+ oxidation state, suggesting a Cl dissociation. The molecular decomposition was not futher discussed. The calculations indicated that the magnetic coupling of the molecular layer on both substrates originates from an indirect exchange mechanism mediated by the nitrogen atoms of the porphyrin ring. The authors claimed that the distance between Fe and the nearest substrate atom is too large for a direct overlap of the interacting orbitals.

This scenario was questioned by Javaid *et al.* [22]. The researchers studied a manganese(II) phthalocyanine (MnPc) molecule adsorbed on a magnetic Co film. They found that also this molecule couples ferromagnetically to the substrate, but on the basis of their DFT calculations and experimental results, claimed that the magnetic exchange is here direct. The computed distance between Mn and Co equals 2.58 Å, and therefore allows for a direct overlap of the corresponding orbitals.

A step forward in the study of magnetic molecules on surfaces was the investigation of FeOEPCl on oxygen-reconstructed Co and Ni films reported by Bernien *et al.* [23]. It was found that the oxygen layer between the molecules and the magnetic film dramatically influences the molecular magnetization: the direction of molecular magnetic moment is antiparallel to the substrate and theoretical calculations predict an antiferromagnetic superexchange interaction between Fe and Co through oxygen.

All the above mentioned studies focus on the molecules adsorbed on fcc(001) substrates. An innovation in this matter is the work by Iacovita *et al.* [16], where cobalt(II) phthalocyanine (CoPc) was placed above Co(111) nanoislands. The magnetization was probed by SP-STM and STS, which give a local information about spin polarization of the Co atom from the molecule. The calculations carried out for this system suggest, that there are two channels leading to the alignment of CoPc spin with the substrate magnetization: direct and indirect (through nitrogens) exchange coupling.

The same molecule (CoPc), but deposited on an iron (Fe) thin film demonstrated very different bahaviour in the work of Brede *et al.* [24]. Theoretical calculations performed for this system suggest that there is a charge transfer from the substrate to the molecule leading to complete quenching of the Co-spin ($S_{Co} = 0$). On the basis of spatially resolved SP-STM measurements the authors proposed that there is a high, locally varying spin polarization present at the whole molecule, but not at Co. These researchers concluded, that progress in the field of molecular spintronics requires a careful design of the whole metal-organic interface and not only a proper choice of the organic molecule.

This opinion is shared by Tsukahara *et al.* [25] who studied iron phthalocyanine (FePc) adsorbed on atomically clean and oxygen-modified copper (Cu) substrates. The authors showed that the strong electronic coupling between Fe and Cu on the metallic substrate quenches the Fe-spin. Only after decoupling the molecule from the surface by

an intermediate layer of oxygen the spin of S=1 in Fe could be restored.

FePc was also extensively investigated by Isvoranu *et al.* [26] by means of XPS. The researchers studied the influence of various ligands binding to Fe on the spin state of this atom judged by the width of the $Fe2p_{3/2}$ XPS peak and theoretical calculations. Whereas the spin of the iron in an undoped FePc equals $S_{Fe} = 1$, the adsorption of pyridine, ammonia (NH_3) and carbon monoxide (CO) results in a complete quenching of the Fe-spin ($S_{Fe} = 0$). Binding with nitric oxide (NO), decreases the Fe-spin by 1/2.

Apart from being a promising medium for magnetic storage devices, organic molecules on surfaces also proved to be potentially useful in a broad variety of applications, like catalysts, sensors, or solar cells. Therefore their properties have been investigated in a series of configurations, e.g.: on metals and on insulators [27–33], self-assembled and randomly distributed [34–38], in densely packed and porous networks [39–43], in chiral and achiral configurations [44–46], in mono-and multilayers [26, 47, 48], etc. These contributions are only a small selection of the broad field of organometallic interfaces.

All the above described articles brought new knowledge into the subject area of (magnetic) organometallic interfaces. The results presented in this thesis emerged from 3.5 years of active research in a very competitive field. Interestingly, in the initial phase of the project, there was little coverage of this branch at international conferences and due to the limited interaction of the few researchers active here, a number of pioneering concepts emerged in parallel from the study of completely different molecular systems. In the past three years, the conference coverage has grown almost exponentially – at the most recent German physical society (DPG) meeting, for example, about 50 abstracts on magnetic molecules were presented. Nowadays, there is a significant flux of research reports, which introduce new views into the field of organometallic interfaces.

In this thesis, I focus on explaining the nature of the magnetic interaction between a monolayer of paramagnetic organic molecules: manganese (III) tetraphenylporphyrin chloride (MnTPPCl) and the ferromagnetic cobalt (Co) substrates. The molecule under study resembles FeOEPCl, for which an experimental and theoretical study was already presented [15]. Although this paper brings valuable information about the nature of the magnetic coupling, the authors failed in the identification of the exact chemical species present on the substrate. The exact chemical species is a significant factor influencing both the adsorption geometry and bonding as well as the electronic and spintronic adsorbate-adsorbent interaction. In this thesis, this deficiency, which was already openly reported in the seminal paper, provided the starting point for a comparative chemical and physical investigation of magnetic molecules upon their adsorption on magnetic substrates. Furthermore, to the best of my knowledge, it is the first PhD thesis reporting on observation of magnetic coupling at room temperature, without an external magnetic field. The essential feature of this study is the use of several complementary surface

science techniques: XPS, LEED and STM as well as XMCD to address surface chemical and surface physical issues next to the most important issue of the magnetic exchange coupling. The experimental techniques used in this work, as well as the sample preparation procedures and characteristics of the studied samples can be found in *Chapter 2*. Various aspects of the organometallic interfaces are presented in the following chapters. First, in *Chapter 3*, the magnetic coupling mechanism of the molecular layer to the substrate is experimentally determined. In this chapter I also show theoretical calculations that help in the identification of the exact constitution of the adsorbate. Following later on, in *Chapter 4*, I compare magnetic, chemical and structural properties of the MnTPPCl molecules adsorbed on two different types of Co substrates: atomically clean and oxygen-reconstructed. Finally, in *Chapter 5*, I address the possibility of a designed spin manipulation on the surface. This last experiment brought us one step closer to potential applications of the organic magnetic layers.

CHAPTER 2

Experimental

In our study of the magnetic coupling at the interface between the molecular layer and the magnetic substrate, we have used specific experimental techniques to obtain information exclusively about the interface. In the first part of this chapter I will present surface science methods used in this study in order to provide the essential basis for later discussion of the results. The second part of this chapter contains a description of the physical and chemical properties of the samples under study.

2.1 Methods

First step toward obtaining atomically clean surfaces required for our experiments is minimization of the influence of all potential sources of contamination i.e. removal of the gas surrounding the sample. According to the kinetic theory of gases, the flux I [$m^{-2} \cdot s^{-1}$] of molecules impinging on the surface from the environment is given by:

$$I = \frac{p}{\sqrt{2\pi m k_B T}} \tag{2.1}$$

where: p – pressure [Pa],
m – mass of the molecule [kg],
$k_B = 1.38$ $m^2 \cdot kg \cdot s^{-2} \cdot K^{-1}$ – Boltzmann's constant, and
T – temperature [K].
Assuming that every particle that hits the surface will remain adsorbed, under normal conditions ($p = 10^5$ Pa, $T = 300$ K, $m_{air} = 29 \cdot 10^{-3} \cdot N_A^{-1}$ kg$\cdot$ mole/mole $= 4.81 \cdot 10^{-26}$ kg)

the surface of 1 cm^2 will be covered within picoseconds (10^{-12} s). To prevent such rapid contamination, surface science experiments in general and also in the specific case of this thesis are performed under Ultra-High Vacuum (UHV) conditions. It means that the residual gas pressure remains in the order of 10^{-5} Pa and below [49]. Pressures indicated in this work will be given in milibars (1 mbar= 10^2 Pa) which is a non-SI unit, but remains to be the most established in the field. UHV conditions, characterized by a considerable lifetime of a fresh sample even under the assumption of a considerable sticking coefficient (≈ 1), start at pressures in the order of 10^{-7} mbar. Vacuum systems for UHV comprise of one or more vacuum chambers coupled to a pumping system including roughing, turbomolecular, ion and sublimation pumps. The following sources give information about the details of creating and maintaining the UHV [49, 50].

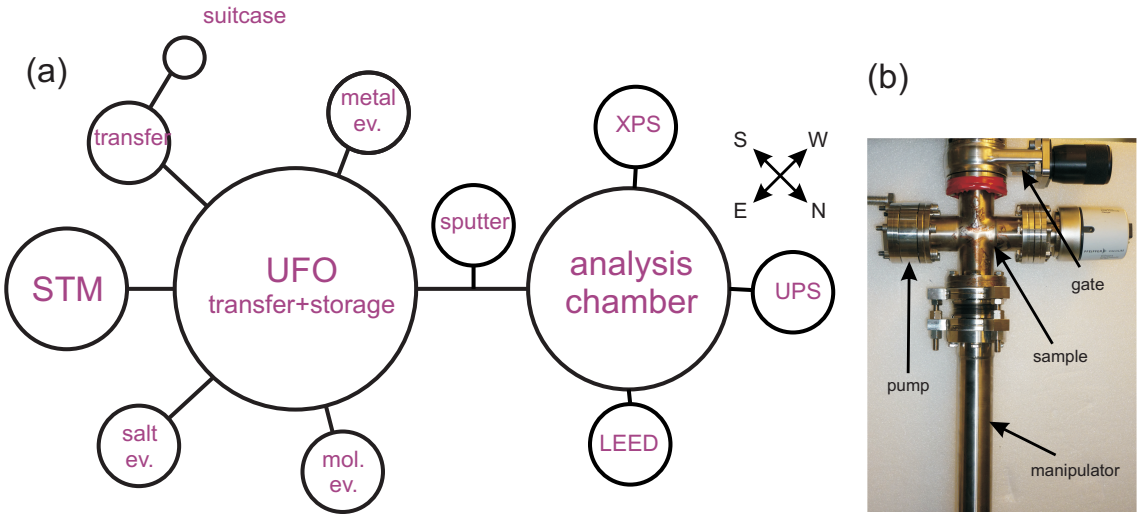

Figure 2.1: The Nanojunction Laboratory at PSI (a) schematic drawing of the multichamber system (the arrows represent geographic directions). **(b)** A photograph of a portable vacuum chamber (vacuum suitcase) used for the sample transfers between NjL and SLS.

All experiments presented in this thesis have been performed at Paul Scherrer Institut (PSI) in two laboratories: the Nanojunction Laboratory (NjL) and at the Surfaces/Interfaces: Microscopy (SIM) beamline of the Swiss Light Source (SLS). NjL hosts a multichamber UHV system with a base pressure of 10^{-11} - 10^{-9} mbar. The central chamber, called "UFO" because of its large, disc-like shape, is used as storage space for up to 32 samples and evaporators. It also serves as a "sample distribution system" to the many other chambers, which are radially attached (see Figure 2.1 (a)). North-west from the UFO chamber there is an analysis chamber which contains monochromatic X-ray and UV sources together with an electron energy analyzer for the photoelectron spectroscopy (XPS and UPS, respectively). In this chamber one can also clean crystals' surfaces by performing sputtering/annealing cycles and determine the surface crystal structure using low-energy electron diffraction (LEED) technique.

South-east from the UFO there is a scanning tunneling microscope (STM) where the surface of the samples at temperatures between 90 K and 300 K can be investigated. Other chambers include evaporation stages for salts, molecules and metals, transfer chambers and a load-lock for introducing new samples. All chambers in NjL are connected through UHV gates so that interchamber transfers can be made without breaking the vacuum. A very important piece of equipment for the presented work is a portable vacuum chamber, also called "vacuum suitcase", displayed in Figure 2.1 (b). It has been used for in-vacuum sample transfers between NjL and the SLS. The pressure in the suitcase is in the order of 10^{-11} mbar due to a special getter pump (SAES). Once activated, this pump does not require an external power supply and maintains low pressure for several weeks. Thanks to this installation, samples could be transferred in the suitcase without a connection to a power supply or battery.

In the next section, several surface science techniques used in the current study will be described in the order in which they are applied during the sample preparation and characterization. It is important to note that the here demonstrated methods are standard procedures used to produce most of the studied samples. However, particular samples investigated in this project required additional treatment, which will be described in detail in the respective experimental chapters.

2.1.1 Surface science techniques

Preparation of atomically clean and flat surfaces studied in this work involves the following processing steps:

1. removing adsorbates and subsequent smoothening of the surface of a single crystal (the substrate), i.e. sputtering/annealing cycles,

2. deposition of thin magnetic films onto the substrate, i.e. electron-beam evaporation, and (in some cases) their subsequent oxidation,

3. molecular deposition.

Sputtering/annealing cycles (1) provide a very efficient procedure of cleaning single crystals. In the sputtering process ions of a chemically inert gas (e.g. argon, Ar^+) impinge on the substrate and cause the ejection of surface atoms. The side effect of this process is roughening of the surface structure and implantation of surface atoms as well as the sputter gas deeper into surface. Cyclic sputtering and annealing assures that defects and impurities are progressively removed. The final annealing restores an atomically clean substrate with well defined surface crystallography. More details about sputtering/annealing process can be found in [50].

After an initial and long (typically 20 cycles or more) cleaning procedure which established the atomically clean substrate, as identified by LEED, samples have been cleaned by performing three sputtering/annealing cycles as detailed in Table 2.1. For this purpose we have used an Omicron sputter gun and a home-built resistive heater (a tantalum wire) mounted on the sample holder. In a series of detailed experiments with different preparation procedures the exact parameters for these three cycles were established. These parameters were shown to reproducibly produce clean surfaces, free of contamination, with homogeneous steps/terraces extending across the whole sample. The cleanness of the samples was monitored by X-ray photoelectron spectroscopy (XPS).

The next step in the sample preparation process is the deposition of the magnetic film (2). For this purpose we have used an electron beam (e-beam) evaporator from Oxford Applied Research. In the e-beam evaporator the high-current electron beam (generated by thermionic emission) locally heats the rod from which the material will be evaporated.

Table 2.1: Parameters of the sputtering/annealing cycles used in the sample cleaning.

Process	Energy [keV]	$P_{applied}$ [W]	Time [min]
Sputter 1	2	-	45
Anneal 1	-	~ 25	20
Sputter 2	1	-	20
Anneal 2	-	~ 25	20
Sputter 3	0.7	-	20
Anneal 3	-	~ 25	20

The magnetic films prepared in our experiments are 20 monolayers (MLs) thick in order to get an in-plane easy magnetization axis and to prevent the substrate atoms from diffusing onto the surface. We have performed the deposition in three steps: (i) evaporation of 10 ML with the sample kept at room temperature, (ii) annealing for 30 minutes, (iii) evaporation of 10 ML, with sample at elevated temperature. The deposition rate was monitored by a 6 MHz Quartz Crystal Microbalance (QCMB) and it was kept between 17 and 25 minutes for various experiments. The cleanness and the thickness of the film were checked by XPS.

For some part of the experiments we have prepared oxidized magnetic films by exposing the 10 ML film to 30 Langmuir (1 L= 10^{-6} torr·1 s= $1.33 \cdot 10^{-6}$ mbar·1 s) of oxygen (O_2). The oxidation step was performed between steps (i) and (ii) and followed by the remaining stages of the procedure. The amount of oxygen was checked afterwards by XPS and LEED. The oxygen layer on top of the initial 10 ML of Co acts as a surfactant for the subsequently deposited Co. The resulting film displays an O-c(2x2) surface reconstruction, as shown in Chapter 4 and in the literature [51]. XPS data reveal that O atoms float on top of the cobalt film.

The last stage of sample preparation is the molecular evaporation (3). Molecules were deposited onto the samples kept at room temperature either from a home-built evaporator or a commercial source (Kentax). In both cases the rate was measured by QCMB and kept around 0.25 ML/min. The stoichiometry of the layer was controlled by XPS and the coverage by scanning tunneling microscopy (STM) and XPS.

After completing of the sample preparation steps 1-3, characterization by XPS (chemical analysis), LEED (surface crystal structure analysis), and STM (topographical analysis) was carried out. In the following paragraphs the three methods will be introduced.

X-ray photoelectron spectroscopy

XPS sometimes also called ESCA (electron spectroscopy for chemical analysis) is a method used for chemical/electronic analysis of the surfaces. The experimental setup consists of three major components: (a) a vacuum chamber, (b) an X-ray source and (c) an electron energy analyzer. The X-rays from the source excite atoms in the sample leading to emission of photoelectrons. The photoelectrons escape from the surface with a certain kinetic energy, which will be analyzed in a spectrometer. The whole process has to be performed in vacuum so that the emitted photoelectrons would be able to travel to the detector without being scattered by gas molecules. Due to the limited inelastic mean free path of the electrons in the sample (usually less than 10 nm for Al Kα X-rays) the method is surface sensitive and therefore suitable for the experiments presented in this work.

In the photoemission process the photon from an X-ray source transfers its energy to a core electron in the sample atom, causing its emission. The sample atom, initially with n-electrons can now rearrange its electron configuration. To get rid of the excess energy either a fluorescent X-ray is emitted or an electron from a higher level (Auger electron) is ejected. All emitted electrons have characteristic kinetic energies (E_K [eV]), that are related to the atomic and molecular environment from which they originated. A binding energy (E_B [eV]) is a potential barrier for an electron caused by Coulomb attraction by a positively charged nucleus. E_B depends on the distance from the nucleus (electronic level) and on the chemical bond formed between the excited atom and its neighbours. From the energy conservation principle we get a straightforward relation between the E_K and E_B:

$$h\nu = E_K + E_B + \phi, \tag{2.2}$$

where: $h\nu$ – the energy of photons in eV (e.g. for Al Kα line $h\nu = 1486.7$ eV),

ϕ – the workfunction [eV] – the minimum energy required to eject an electron from the highest occupied level into vacuum.

Because of the electron emission it is important that the sample is conductive and

grounded to maintain a constant supply of the missing electrons. Insulating samples can also be studied by XPS, but the setup should be equipped with an additional electron gun, which would compensate for the charging of the sample [49].

An XP spectrum contains information from all stages of the physical process: the initial (with n-electrons) and the final (with (n-1) electrons) states. The initial state is the ground state of an atom before photoemission. Its presence in the XP spectrum is observed as a chemical shift of E_B due to formation of chemical bonds with the surrounding atoms. The final state effects can cause additional features to appear in the spectrum. Such features involve shake-up satellites, modified peaks by an added background originating from inelastic scattering background or Auger peaks. Among the final state effects spin-orbit coupling is particularly important to note as it causes splitting of specific photoemission peaks. If an electron is photoemitted from a 2p level, then the remaining electron can exist either in a spin-up ($s = +1/2$) or in a spin-down ($s = -1/2$) configuration. Those two possible states have the same energy i.e. they are degenerate. A magnetic interaction between those states (up or down) and their orbital momenta (l) may lead to the splitting of the degenerate states, called spin-orbit coupling (ls coupling). This splitting is characterized by the quantum number: $j = l \pm s$ and can be observed e.g. for Cu2p lines ($l = 1$) where the two peaks are $j = 3/2$ at 932.7 eV and $j = 1/2$ at 952.5 eV [52].

In the NjL XPS is performed using Focus 500 (Specs) monochromatic Al Kα X-rays (since summer 2009) and a Phoibos 150 (Specs) hemispherical energy analyzer with eight channel electron multipliers (channeltrons) used for the detection of electrons.

After completing the chemical analysis of the sample we can proceed to the determination of the crystal structure of the surface.

Low-energy electron diffraction

LEED provides structural information about the surface crystal lattice. According to the formula of de Broglie a wavelength λ [m] of an electron is calculated from the expression:

$$\lambda = \frac{h}{\sqrt{2mE}},\ \lambda = \sqrt{\frac{150}{E}}, \tag{2.3}$$

where: h – Planck's constant, $h = 4.14 \cdot 10^{-15}$ [eV·s],
m – mass of an electron, $m = 9.11 \cdot 10^{-31}$ [kg],
E – energy of an electron [eV].

In the typical range of energies used for LEED ($E < 200$ eV) the wavelength of electrons fulfilling the diffraction condition is in the order of interatomic distances. Additionally, the mean free path of low-energy electrons is very short ($5 - 10$ Å). That is why the method is highly suitable for the determination of the 2D crystal structure of the surface.

The interpretation of the diffraction pattern relies on the concept of the reciprocal space, in which the Fourier transform of a spatial function is represented. A simple example of a surface reconstruction on an fcc(001) lattice in real and reciprocal space is displayed in Figure 2.2. Arrows a_1 and a_2 represent the lattice vectors of the fcc(001) structure; b_1 and b_2 – of the reconstruction. The arrows with asterisks represent the respective reciprocal lattice vectors. As seen in the left panel of Figure 2.2 the same overlayer structure can, in this case, be described by two equivalent Wood's notations: $R45°(\sqrt{2} \times \sqrt{2})$ or $c(2 \times 2)$. Wood's notation is straightforward and is derived from the following relation:

$$\frac{b_1}{a_1} \times \frac{b_2}{a_2}. \tag{2.4}$$

The $R45°(\sqrt{2} \times \sqrt{2})$ notation represents a primitive cell and its lattice vectors can be directly related to the reciprocal space, but the advantage of the $c(2 \times 2)$ notation is that it is more intuitive.

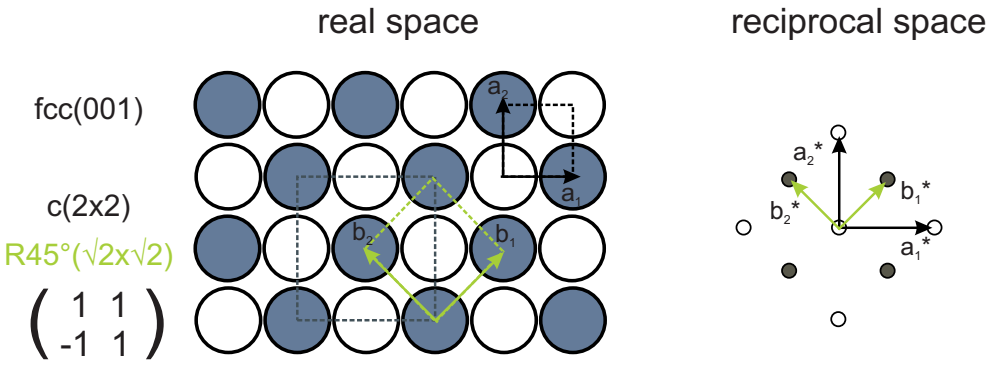

Figure 2.2: An example of a superstructure in real and reciprocal space. Black (a_1 and a_2) and green (b_1 and b_2) arrows represent the substrate and the superstructure lattice, respectively. The Wood and matrix notations of the reconstruction are given on the left. The LEED pattern and respective reciprocal vectors (a_1*, a_2*, b_1* and b_2*) are displayed on the right.

Although the Wood's notation is a valuable tool for describing the surface reconstruction, its applicability is limited to those cases where the angle between b_1 and b_2 is the same as between a_1 and a_2. For more complex overlayer structures it is therefore advisable to utilise the more general matrix notation. The reconstruction matrix M is defined as follows:

$$\begin{pmatrix} \vec{b_1} \\ \vec{b_2} \end{pmatrix} = M \begin{pmatrix} \vec{a_1} \\ \vec{a_2} \end{pmatrix}. \tag{2.5}$$

For the example in Figure 2.2:

$$M = \begin{pmatrix} 1 & 1 \\ -1 & 1 \end{pmatrix}.$$

The LEED equipment used in our study (Omicron) consists of the LEED optics, a fluorescent screen, an electron source and a camera for recording the patterns. The electron source is located between the camera and the fluorescent screen, hence it is visible on the images covering the (0, 0) spot.

Scanning tunneling microscopy

STM is a widely used method for imaging of the topography of surfaces, among many other surface properties which can be mapped. Its advantage over LEED is the acquisition of real-space images also of non-periodic structures at surfaces. Uniquely, STM can visualise the individual molecules in an unordered molecular layer.

The method relies on quantum tunneling as first described by Schrödinger (details can be found e.g. in [53]). Grace to this effect, an electron wave function can penetrate into a potential barrier. If the potential barrier is relatively narrow (in the order of a few Å) then an electron can pass from one side to the other (Figure 2.3). The tunneling current (I_t [A]) depends exponentially on the width of the barrier (d [nm]) [50, 53]:

$$I_t = f(U)exp(-2\kappa d), \tag{2.6}$$

where: U – applied bias voltage [V],

$f(U)$ – function of electronic structure of the sample and the tip [A],

$\kappa = \sqrt{\frac{2m\varphi}{\hbar^2}} = 5.1\sqrt{\varphi(eV)}$ nm^{-1} – a decay constant,

φ – effective barrier height, $\varphi \approx \frac{\varphi_1+\varphi_2}{2}$ [eV], φ_1 and φ_2 are the workfunctions of the sample and the tip, respectively (see Figure 2.3).

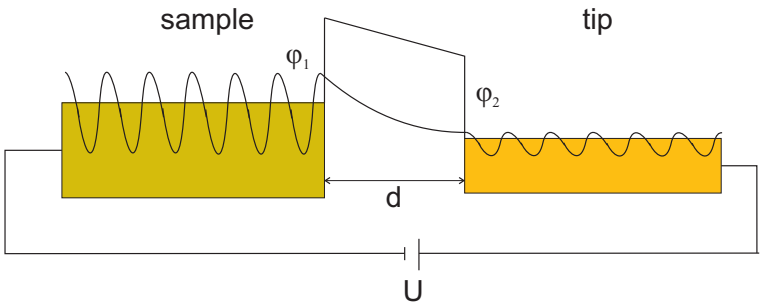

Figure 2.3: A quantum-mechanical principle behind the scanning tunneling microscopy. Tunneling of the electron wavefunction through a potential barrier of the width d. φ_1 and φ_2 are the workfunctions of the sample and the tip, respectively; U is the applied bias voltage.

The consequence of the exponential decay of the tunneling current (Equation 2.6) is that within a microscope, where a tip is held in close proximity to the substrate surface, the tunneling occurs from/to the outermost atom(s) of the tip. Therefore atomically

sharp tips are an essential part of a successful experiment. In the NjL we use tungsten (W) tips produced by electrochemical etching in a 2 molar (M) solution of sodium hydroxide (NaOH). The prepared tip is first imaged in a scanning electron microscope (SEM) to make sure, that it is sufficiently sharp in its overall macroscopic shape. In fact, a perfect STM tip should have a single atom at the apex (diameter in the order of Å), what cannot be judged from an SEM image (resolution $\sim$ 5 nm). Therefore SEM only provides a rough idea of the quality of the tip. Later on, tips are sharpened by in-situ sputtering and by performing additional sharpening procedures, e.g. high-field treatment or controlled collision with a sample [53]. The tip is mounted in the piezoelectric scanner, which is controlled by a computer. A conductive sample is fixed in a holder and grounded. In order to accelerate electrons between the sample and the tip, a high voltage is applied to the tip. Because of the very small tip-sample distances required for the imaging mechanism by quantum-mechanical tunneling, the microscope is very sensitive to vibrations. In order to obtain good images the whole setup needs to be suspended and all vibrations should be damped. During scanning, the feedback loop controls the tip-sample distance in that it retracts or approaches the tip in order to keep the tunneling current constant.

The contrast in the STM originates from the changes in the tunneling current, which in turn, depends on the electronic structure of the sample and of the tip as well as on the states available for tunneling or field emission. The quantity $f(U)$ from Equation 2.6 contains information about the local density of states (LDOS) of the sample and the tip. It plays a crucial role in the determination of the I_t and therefore one can think of an STM as a measurement of the LDOS or local electronic structure of the sample, after it has been experimentally verified that the tip exhibits electronic states which are dominated by "free electrons" and does not contain strong density of states features.

Besides the capability of acquiring topographical and electronic density of states data, STM can also provide information on the spin-dependent density of states, i.e. on surface magnetism. The so-called spin-polarized STM (SP-STM) has been developed since the first publication in 1990 [54] and has been successfully used in many newer studies to provide a spin-dependent contrast [16, 55].

The STM setup installed in the NjL is a low temperature STM from Specs, the so-called "Aarhus STM" (set up in spring 2010). It provides very high mechanical and thermal stability for temperatures ranging from 90 K to 400 K and for scanning at rather high rates for the frame.

2.1.2 Magnetic interactions: X-ray magnetic circular dichroism

XMCD is one of the experimental methods which exploit synchrotron light. Due to this fact, before explaining principles of XMCD, I will introduce the most important

features of the synchrotron radiation. Particularly, the Swiss Light Source (SLS), where the experiments were carried out, will serve as a representative example. In the second part of this section I will describe possible magnetic interactions, followed by the details of the XMCD technique.

Synchrotron radiation

The main advantages of the synchrotron light over conventional (laboratory) sources include high brightness and high intensity, wide energy spectrum and the possibility of choosing a suitable wavelength ranging from infrared to hard X-rays. Synchrotron light is polarized, monochromatic, and pulsed. Historically, the first synchrotrons, built in 1940's, were designed for accelerating particles to very high energies and the radiation was an unwanted by-product that caused energy losses. In 1956 the first experiment using "parasitic" synchrotron radiation was performed at Cornell University [56]. Nowadays, there are around 50 facilities in the world used as sources of synchrotron radiation [57]. One of them is the Swiss Light Source (SLS). In the SLS the electrons of 2.4 GeV energy and constant velocity close to the speed of light ($v \sim c$) circle around a 288 m circumference storage ring. They are accelerated by a microwave radiofrequency and are formed by focusing magnets into electron bunches. Therefore the radiation generated by their radial acceleration in the magnetic field of bending magnets or undulators consists of pulses. SLS hosts 18 beamlines dedicated for various fields of research, like: physics, biology, medicine or materials science. In general, there are two kinds of beamlines in the SLS depending on the source of radiation: (i) bending magnet (ii) insertion device. If the electron bunch travels through a bending magnet, it will be deflected from its linear trajectory and experience a centripetal acceleration. The radiation will be emitted along the velocity vector, i.e. tangentially to the electron path. It was calculated [58] that, in the resting observer's frame of reference, the light is radiated into a cone and the most of the radiation is contained within an opening angle of $\frac{1}{\gamma}$, where $\gamma = [1 - \frac{v^2}{c^2}]^{-1}$. Additionally, the radiation from a bending magnet can be linearly or circularly polarized (for details, see [58]).

Insertion devices are inserted into straight sections of a storage ring. There exist two types: wigglers and undulators, but only the latter are used in the SLS. Undulators consist of an N number of electromagnets with electron bunches being guided through the gap. In this arrangement, the electrons are forced into an oscillatory (or helical) path around their propagation direction. Each electron bunch passing through the magnetic field in the gap will emit radiation at each of the individual electromagnets and will thereby emit light in a specific phase relation of the specific position. This light will constructively interfere with itself and therefore the spectrum of an undulator consists of peaked harmonics. The intensity of radiation from an undulator is improved by a

factor of N over a bending magnet and the emission angle is narrower by $1/N$. As a result, the spectral brightness [59] of an undulator[1], compared to the spectral brightness of a bending magnet is improved by a factor of N^2. Additionally, one can control the polarization of light coming from an undulator much better than that coming from a bending magnet, which is an important advantage for the XMCD technique.

The experiments presented in this work were carried out at a two-undulator beamline allowing for the very precise and time efficient switching of the polarization of X-rays. The beamline is dedicated for magnetic measurements: XMCD spectroscopy and magnetic microscopy.

Magnetic interactions

In a quantum mechanical approach an electron in an atom can be described by a set of four quantum numbers (qn's): (i) the first (principal) qn describes an electron shell, $n = 1, 2, 3, \ldots$ (ii) the second (azimuthal) qn describes a subshell or an angular momentum of an electron, $l = 0, 1, 2, \ldots, (n-1)$, (iii) the third (magnetic) qn describes an orbital, i.e. the projection of the angular momentum, $m_l = -l, \ldots, -2, -1, 0, 1, 2, \ldots, +l$) and (iv) the fourth (spin) qn describes the spin projection, $m_s = +1/2$ or $-1/2$. The source of magnetization in materials is an orbital and spinning motion of an unpaired electron around the nucleus (Figure 2.4 (a)). The motions give rise to an orbital (m_l) and a spin (m_s) magnetic moments, respectively. The total magnetic moment of an electron (m_{tot}) is the sum of both contributions:

$$\vec{m_{tot}} = -\mu_B(\vec{l} + 2\vec{s}). \tag{2.7}$$

Quantity μ_B is a Bohr magneton and it amounts $\frac{e\hbar}{2m_e} = 9.27 \cdot 10^{-24}$ [A·m^2]. It is often used as a unit of a magnetic moment. $\vec{l}$ and $\vec{s}$ are respectively, orbital and spin angular momenta.

Magnetic ordering is a consequence of the interaction between magnetic moments. The most important magnetic interactions for this work are the exchange interactions originating from two mechanisms involving electrons in matter: the Coulomb repulsion and the Pauli exclusion principle. Quantum-mechanical considerations of an interaction between two electrons with spins s_i and s_j provide the exchange Hamiltonian in a form:

$$H = -2J_{ij}s_i s_j, \tag{2.8}$$

where J_{ij} is energy of the exchange interaction.

[1] Spectral brightness is defined as the photon flux emitted per unit source area per unit radiation opening angle

The exchange energy removes the degeneracy of the spin-up and spin-down half bands leading to unequal occupancy of those states. This results in a creation of a net magnetic moment. If the two electrons are close enough so that their wavefunctions can overlap, the exchange interaction between them is called a direct exchange [58, 60, 61]. In case the two electrons are too far away for their orbitals to overlap, then the magnetic coupling can occur through a mediating atom leading to an indirect exchange. A particular case of an indirect exchange is the superexchange interaction. It is often observed in transition metal oxides, where the 3d magnetic ions are separated by a 2p oxygen ion. The electron configuration of the oxygen atom is $1s^2 2s^2 2p^4$, so one of the 2p orbitals is empty (a diamagnetic oxygen atom). Thus, it is possible for the metal 3d electrons to be partially delocalized on oxygen 2p orbitals. Due to the exclusion principle, the two electrons residing on one orbital cannot have the same spin; therefore the alignment is antiparallel, i.e. antiferromagnetic (see Figure 2.4 (b)).

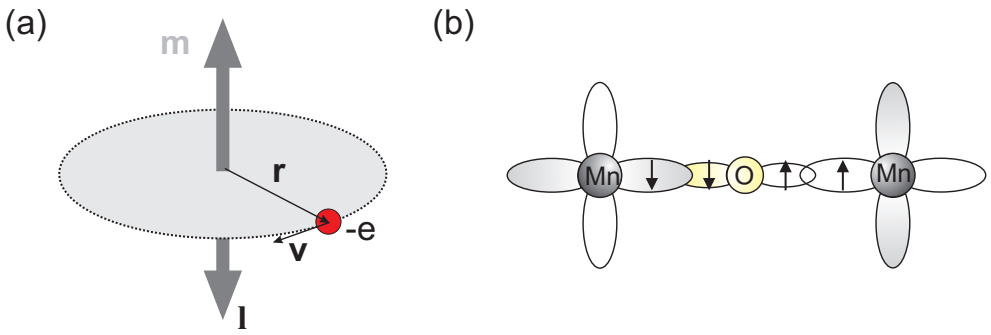

Figure 2.4: Magnetic interactions (a) magnetic moment originating from an orbital motion of an electron. **(b)** illustration of the antiferromagnetic superexchange coupling between two Mn atoms mediated by oxygen.

The last mechanism that belongs to the exchange interaction family is the double exchange interaction. It is considered in systems, where several 3d ions are in different valence states. Such a condition is not fulfilled for the systems studied in this thesis.

It is important to note, that in 3d ions a large ligand field eliminates the degeneracy of the d orbitals. Due to this fact the main contribution to the total magnetic moment comes mostly from the spins. Another effect of the large ligand field is the possibility for violation of Hund's rules leading to intermediate- or low-spin states that can sometimes be diamagnetic [61].

X-ray magnetic circular dichroism

XMCD relies on the X-ray absorption spectroscopy (XAS) in which the X-rays from a synchrotron source excite atoms in the sample and cause core-to-valence electron transition. This transition is manifested in X-ray absorption edges, which occur at certain

photon energies and are characteristic for different elements. The circular dichroism in the XMCD is computed as the difference of two absorption spectra acquired with right- and left- circularly polarized X-rays (see Figure 2.5 (a) and (b)). These two polarizations of the incident X-ray beam carry opposite photon spins: $+\hbar$ (circ+) and $-\hbar$ (circ-), respectively. The opposite photon spins interact differently with the core electrons of the excited species. XMCD is usually observed in $2p \rightarrow 3d$ transitions and can be considered as a two-step process. In the first step, the photons transfer their angular momentum to the electrons. Because the 2p level is split into $2p_{3/2}$ (L_3) and $2p_{1/2}$ (L_2) peaks (Figure 2.5 (a)) due to spin-orbit coupling, the photon spin is partially transferred to the electron spin, i.e. the electrons will be spin-polarized[2]. The spin polarization will be opposite for L_3 and L_2 edges, because the spin-orbit coupling is also opposite ($l+s$ and $l-s$, respectively). The effect of magnetization is visible in the second step. The valence shell (3d) of magnetic atoms is split due to the exchange interaction and the electron population of spin-up and spin-down states is not equal. When the photon angular momentum (or the excited electron spin) is aligned with the magnetization direction, i.e. with the excess electron population in the 3d shell, then the probability for excitations is the highest and consequently the maximum X-ray absorption signal is obtained. A schematic drawing of the absorption event in a 3d metal is displayed in Figure 2.5 (d).

The major advantages of XMCD are the elemental specificity and surface sensitivity. Notably the sensitivity of XAS/XMCD also allows for the identification of atoms in different oxidation states by their different population of the electron shells. The surface sensitivity of XMCD relates to the measurement of the cumulated current of photoemitted electrons in the total electron yield (TEY) mode. This mode exclusively depends on the photoemission processes within a surface proximal layer characterized by the "escape depth" corresponding to the kinetic energy of the photoelectrons. Note that photoemission process can occur far deeper inside the sample, but only leads to recombination and will not be contributing to the TEY measurement. XMCD spectrum can be quantitatively analysed for the relative contribution of spin- and orbital magnetic moments by using sum-rules.

The sum rules, described by Thole *et al.* [63] and Carra *et al.* [64], are a procedure for the calculation of orbital (m_o) and spin (m_s) magnetic moments from the XMCD data. It was shown by Chen *et al.* [65], that the sum rules in a form:

$$\begin{aligned} m_o &= \frac{-4q(10-n_{3d})}{3r} \\ m_s &= \frac{-(6p-4q)(10-n_{3d})}{r} \end{aligned} \tag{2.9}$$

where the p, q and r values are integrals indicated in Figure 2.5 (b) and (d) and n_{3d} is the 3d electron occupation number, agree very well with gyromagnetic ratio measurements

[2]This is an effect, which was first described by U. Fano [62], called after him.

for Co and Fe thin films. On the other hand, Piamonteze *et al.* [66] show that for $3d^4$ (e.g. Mn^{3+}) and $3d^5$ (e.g. Mn^{2+}) species the sum rules give an error of around 30-50% and the calculations of the magnetic moments are therefore meaningless. Because Mn ions are in the focus of this work, we have developed a different experimental method for accessing their spin configuration, than the sum-rules.

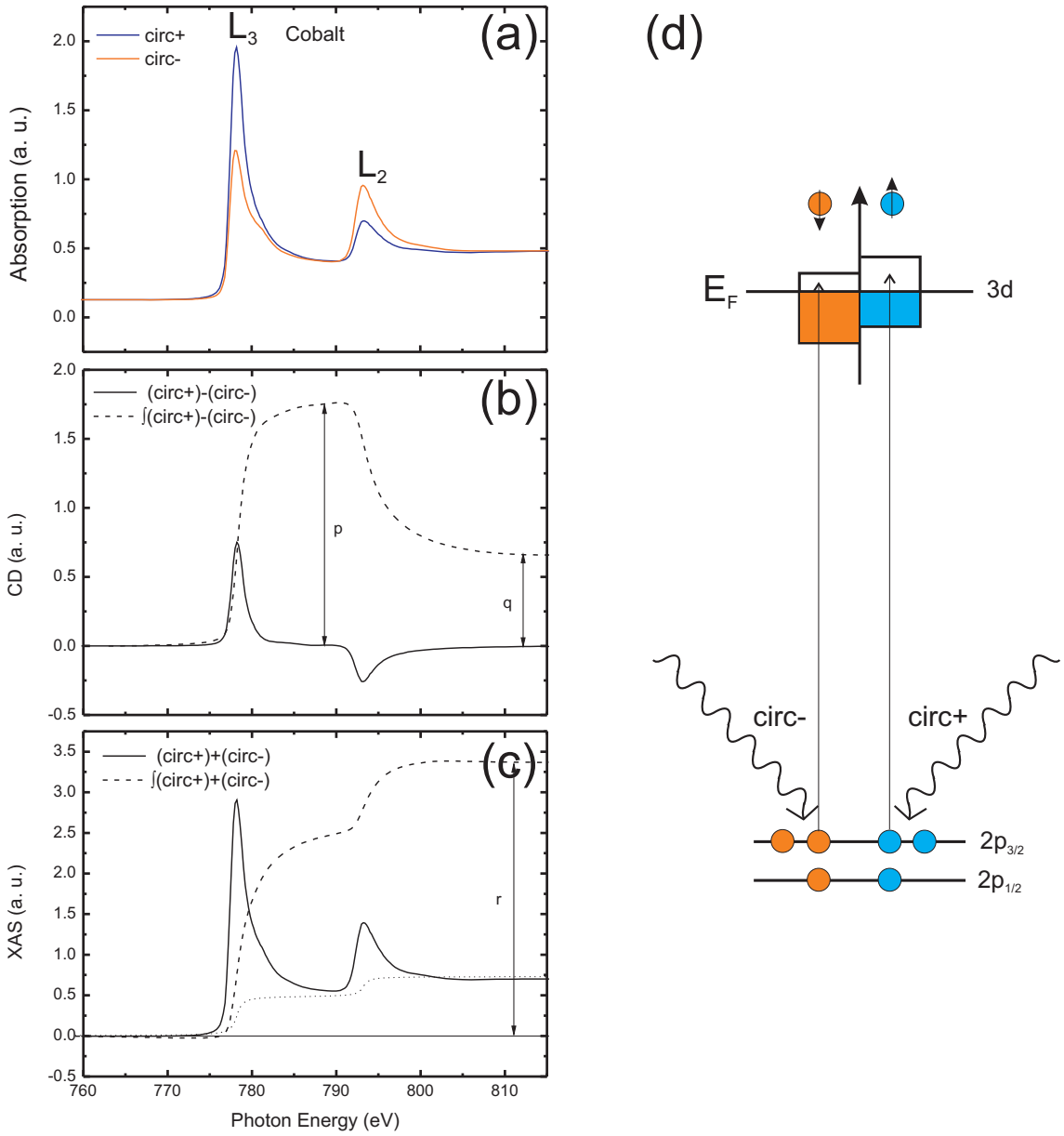

Figure 2.5: L-edges absorption and dichroic spectra of cobalt. **(a)** absorption of circularly polarized X-rays, **(b)** dichroic spectrum and the integral, **(c)** sum of absorption spectra, the two-step background and the integral. p, q and r values are used for sum-rules analysis, **(d)** illustration of the absorption of circularly polarized photons in a 3d magnetic element.

The XMCD measurements for this thesis were carried out at the SIM beamline of the

SLS. The samples prepared in the NjL were transported to SIM in UHV in a vacuum suitcase. The beamline provides high brilliance soft X-ray light in the energy range of $130-2000$ eV from two elliptical twin undulators, which permit switching of the photon helicity optically within a few seconds [67]. All spectra were recorded at room temperature and normalized to the incident photon flux. An external magnetic field of ~ 125 militesla (mT) was applied before the measurement parallel to the surface plane of the sample to assure in-plane single-domain magnetization of the thin film. The L-edges absorption spectra for substrate and adsorbate were recorded in grazing incidence ($\sim 20°$) in TEY mode in remnant magnetization of the substrate. To obtain XMCD spectra one has to subtract XA spectra of either opposite photon helicities or acquired with opposite directions of the external magnetic field. Both are possible at SIM beamline, therefore to avoid confusion, all XMCD spectra showed in this thesis (except the ones explicitly specified) were recorded with the same substrate magnetization direction. Additionally, the XMCD and XA spectra have been scaled by the same factor to give the XAS peak heights of unity.

2.2 Materials

In the presented experiments organic molecules are sublimed onto thin cobalt films grown on copper single crystals (Co/Cu(001)). The details of the sample preparation are explained in Section 2.1.1. In the following two sections I will describe the properties of the substrates and of the adsorbates in physico-chemical details.

2.2.1 Organic molecule

As adsorbates we have used an organometallic complex: manganese (III) tetraphenylporphyrin chloride (MnTPPCl) presented in Figure 2.6 (a). It consists of a manganese (Mn) ion coordinated by four pyrrole nitrogen (N) atoms and one chlorine (Cl) atom [68]. The axially coordinated Cl introduces an electric dipole moment $Mn^{\delta+} - Cl^{\delta-}$, influencing the adsorption scheme, similarly to the case of chloro[subphthalocyaninato]boron(III) (SubPc) molecule [69]. The four phenyl rings are usually rotated by 90° with respect to the molecular plane, but it has been shown [70], that this angle is flexible upon adsorption on a surface. The planar shape of the molecule in vacuum was computed by DFT calculations to be square with a dimension of 1.24 nm.

The Mn ion, surrounded by five atoms (4 N and 1 Cl) is in 3+ oxidation state and contains four electrons in the 3d levels. A square pyramidal crystal field acting on Mn cancels degeneracy of the Mn 3d levels and results in splitting shown in Figure 2.6 (b) (adapted from [4]). The lowest in energy are the orbitals, which do not point directly towards the ligands (in Figure 2.6(b) the ligands are assumed to lie along the

xyz axes). The orbitals: d_{xz} and d_{yz} are degenerate as their geometry and the alignment towards the Cl ligand (along the z axis) are very similar. Slightly higher in energy is the planar d_{xy} orbital which points inbetween the four N ligands. Accordingly, the d_{z^2} and $d_{x^2-y^2}$ are the highest in energy, pointing directly at Cl and the four N, respectively. In bulk MnTPPCl, the electron configuration of the Mn ion is high-spin, i.e. all 3d levels (except for the $d_{x^2-y^2}$) are singly occupied resulting in $S_{Mn} = 2$ [71]. When adsorbed on a surface, the splitting of Mn 3d levels and their occupancy might change. In particular, the lowest orbitals: d_{xz}, d_{yz} and the slightly higher d_{xy} lie very close in energy, therefore one cannot exclude interchanging of their relative energy positions. A more detailed discussion on this subject will follow in Chapter 4.

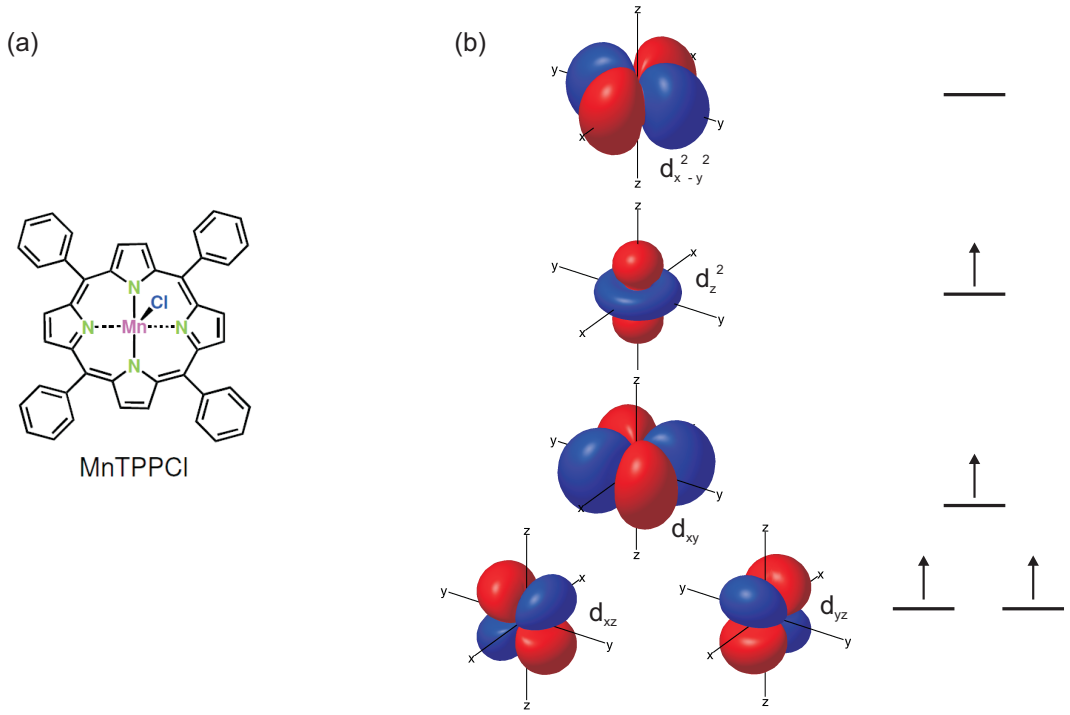

Figure 2.6: MnTPPCl molecule and the crystal field splitting of the Mn 3d levels. **(a)** Scheme of the molecule under study; **(b)** splitting of the Mn 3d levels caused by the interaction with five ligands in square pyramidal geometry: shape of the 3d orbitals and their electron filling.

Crystal field theory (CFT) assumes that the ligands are point charges and that the metal-ligand bonding has purely ionic character. In reality however, there is an overlap of metal and ligand orbitals and the electrons from both elements can be delocalized. Additionally, type of a ligand is also an important factor influencing the splitting of the 3d levels. These modifications are accounted for in ligand field theory (LFT), which gives a better agreement between the predictions and experimental observations than the CFT. We should note however, that all the models derived from various theories are only close to reality and experiments very often deviate from the predicted behaviour.

2.2.2 Substrates

The substrates, on which we evaporate organic molecules, play a crucial role in the experiment. Firstly, they accommodate the molecules and therefore have to provide large terrace sites and must not contain random impurities which could influence the adsorption. Secondly, and even more important, substrates are the source of magnetization for the adsorbates, that is why we have to make sure that our thin films can be magnetized in single domains by the externally applied magnetic field. In our experiments ferromagnetic cobalt films are grown on copper (001) single crystals bought from Mateck. Round Cu crystals are 2 mm thick and have a diameter of 8 and 10 mm (two crystal sizes were used).

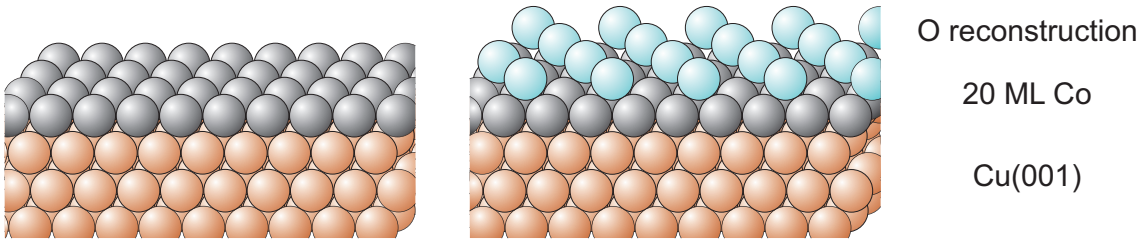

Figure 2.7: Co thin films used as substrates. Cartoons of an atomically clean (left) and oxygen-reconstructed Co (right). The sizes of atoms and the thicknesses of layers are not in scale.

20 ML ($\approx$ 3.5 nm) thick Co film on Cu(001) single crystals grows in a layer-by-layer mode into an fcc(001) structure and its easy magnetization axis is parallel to the surface [72]. In part of the experiments we have intentionally introduced surface impurities by performing a controlled oxidation of the Co film, described in Section 2.1.1. The resulting substrate exhibited new structural and magnetic features (Figure 2.7), which are explained in detail in Chapter 4. Another modification of the Co substrate was an induced roughness of the Co film. On such a rough surface, the molecules were forced to adsorb at the kinks and steps, which influenced the magnetic coupling. This experiment as well as the preparation procedure of the rough films are described in Chapter 3.

CHAPTER 3

Indirect coupling of the Mn-porphyrin to the ferromagnetic Co substrate[1]

Organic molecules adsorbed on ferromagnetic surfaces have been shown to couple magnetically to the substrate allowing for magnetic ordering at room temperature [14, 15, 23, 37]. The mechanism of the exchange coupling is influenced by the strong substrate-molecule interaction and crucially depends on the bonding between the substrate and the molecule. A detailed knowledge on the interactions at the interface is an important prerequisite for the extensive analysis and the future design of the electronic and magnetic interface properties. For the here studied MnTPPCl/Co(001) system two important cases can be discriminated, i.e. the *direct exchange* coupling of orbitals containing unpaired electrons with the electronic system of the substrate, and the *indirect exchange* coupling where the magnetic response derives from an intermediate atomic species linking the unpaired electron system in the molecule with the ferromagnetic substrate electrons.

In this chapter we present experimental evidence for the mechanism of magnetic coupling of a MnTPPCl molecule to a pre-magnetized Co thin film. We complement the experiments by density functional theory (cluster DFT and DFT+U) calculations, investigating the coupling of manganese porphyrin chloride (MnPCl) to a Co surface. Additionally, we try to resolve the question about chlorine dissociation, by comparing experimental data with the theoretical calculations. A combination of XMCD with complementary surface analysis, in particular STM and XPS, provides detailed information about the chemical species adsorbed on the surface as well as an assessment of molecular orientation.

[1] The results of this chapter were published in *Journal of Physical Chemistry C* **115**, 1295 (2011).

To experimentally verify the magnetic coupling mechanism for the MnTPPCl molecule, we have evaporated it onto atomically smooth (step defect poor) and rough (step defect rich) Co films and compared the respective normalized XMCD signals at the Mn L-edges. The minimum spacing between Mn and Co in an assumed planar molecular orientation on the surface is calculated to ~ 3.67 Å (discussed below). This distance is too large for the overlap between the 3d orbitals of Mn and Co to occur and therefore direct exchange coupling between Mn and Co is not probable. On the basis of this assignment, the direct exchange coupling between MnTPPCl and the Co film would become more dominant in the case of selective adsorption of molecules on steps or kinks of the substrate, where porphyrins tend to adsorb preferentially, due to the generally more favorable physical and/or chemical interaction of the π-system with the substrate atoms at closer proximity [70, 73]. In this case, only the proportion of molecules adsorbed on defects is expected to contribute to the observed circular dichroism. The present study aims to resolve this issue by investigating the magnetic coupling by XMCD spectroscopy and the adsorption geometry on the rough and smooth ferromagnetic substrates by STM. All measurements have been carried out in UHV at room temperature.

3.1 Smooth vs. rough substrate – experimental results

Smooth Co films were prepared according to the procedure described in Chapter 2. The rough substrate was produced by sputtering the smooth Co with Ar^+ ions of 0.7 keV energy for 2.5 min. No annealing step was performed afterwards. The substrates can be clearly distinguished on the basis of their surface morphologies mapped by the STM (Figure 3.1). While the smooth Co films are characterized by broad, rounded terraces with very few defects, the rough surface contains grooves, which form a characteristic "wrinkled" shape. The original morphology of the Co as deposited before sputtering can be still recognized by the round terrace shape. Differences between the two substrates can be clearly quantified from the respective height profiles in Figure 3.1, which were taken along the lines depicted in the corresponding STM images over a distance of ~ 50 nm. One can clearly identify the two flat terraces ~ 20 nm wide in the surface profile corresponding to the smooth sample, whereas in the case of the rough sample the height profile is much more corrugated indicating far narrower flat areas (~ 3 nm wide).

MnTPPCl molecules were thermally sublimed onto the magnetized Co films with smooth or rough morphologies and in the following study two molecular coverages were investigated: 0.3 and 0.9 ML (monolayers). The XPS data obtained for a thick layer of MnTPPCl molecules (≈ 10 ML) revealed a ratio of 44.1 : 4.0 : 0.9 between C:N:Cl atoms which compares well to the chemical mass formula of MnTPPCl ($MnC_{44}N_4H_{28}Cl$), and thus indicates, that molecules stay intact during the evaporation process. The molecular

integrity of the MnTPPCl molecules before and after the evaporation was also confirmed by a UV-Vis spectroscopy (data shown in Chapter 4 and in [37]).

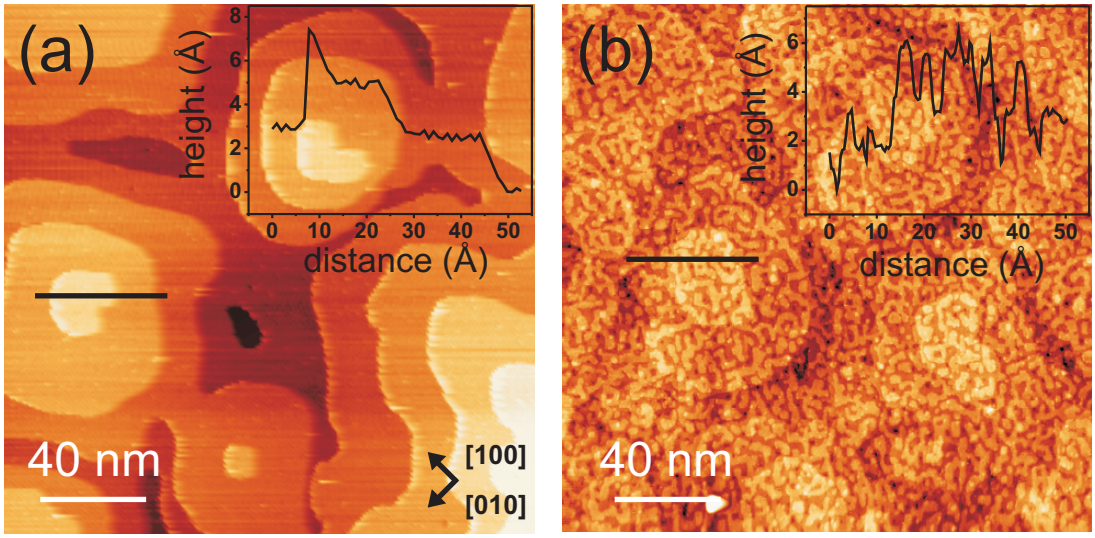

Figure 3.1: 2D STM images of "smooth" and "rough" preparations of the Co substrates. (a) "smooth" (I = 0.12 nA, U = - 2.5 V) and **(b)** "rough" (I = 0.25 nA, U = - 1.4 V) 20 ML thin Co films on Cu(001). Insets present respective height profiles along the ∼ 50 nm long lines depicted in the images. The crystallographic directions of the substrate are the same in both images and are indicated by the arrows in (a).

The shape of the molecule in the STM images is cross-like and the in-plane dimensions are calculated by DFT to be 1.24×1.24 nm^2. It is worthwhile to note that the phenyl substituents are oriented out of the porphyrin plane due to a steric repulsion mechanism [74]. In a previous study of MnTPPCl [14] it was shown by near-edge X-ray absorption fine structure spectroscopy (NEXAFS) [75], that these molecules lie flat on the Co substrate. In the present work, STM images of MnTPPCl molecules on both smooth (Figure 3.2 (a)) and rough (Figure 3.2 (b)) magnetized Co films confirm the adsorbed flat-lying configuration of the MnTPPCl molecules on the surface. The size of the molecule measured in the STM is $\sim 1.17 \times 1.33$ nm^2, which is in good agreement with the calculated value. The rectangular shape might be associated with the conformational flexure of the porphyrins along the dihedral phenyl-porphyrin bond [74].

On the smooth Co substrate (Figure 3.2 (a)) the molecules (coverage 0.9 ML) are adsorbed in a random fashion and do not apparently occupy preferred adsorption sites, indicating a significant substrate-molecular interaction which retards self-assembly of the layer. Similarly, on the rough surface, where the displayed coverage is much smaller (0.3 ML, Figure 3.2 (b)), the molecular adsorption also appears random. This observation can be explained by the considerable bonding strength and the correspondingly low diffusion of MnTPPCl on the Co substrate upon deposition and relaxation. Additionally to the well defined cross-shaped molecules on the rough surface, we can also distinguish

a significant number of isolated protrusions in Figure 3.2 (b). We tentatively assign these structures to the products of a molecular decomposition process on the substrate, possibly chlorine. This assignment is supported by the earlier reported evidence that molecules adsorbed on metals undergo dissociation leading to the removal of Cl atom, which remains bound to the substrate [37, 76]. On the smooth Co surface shown in Figure 3.2 (a), such protrusions are also observed, but they are less apparent due to the almost full monolayer coverage.

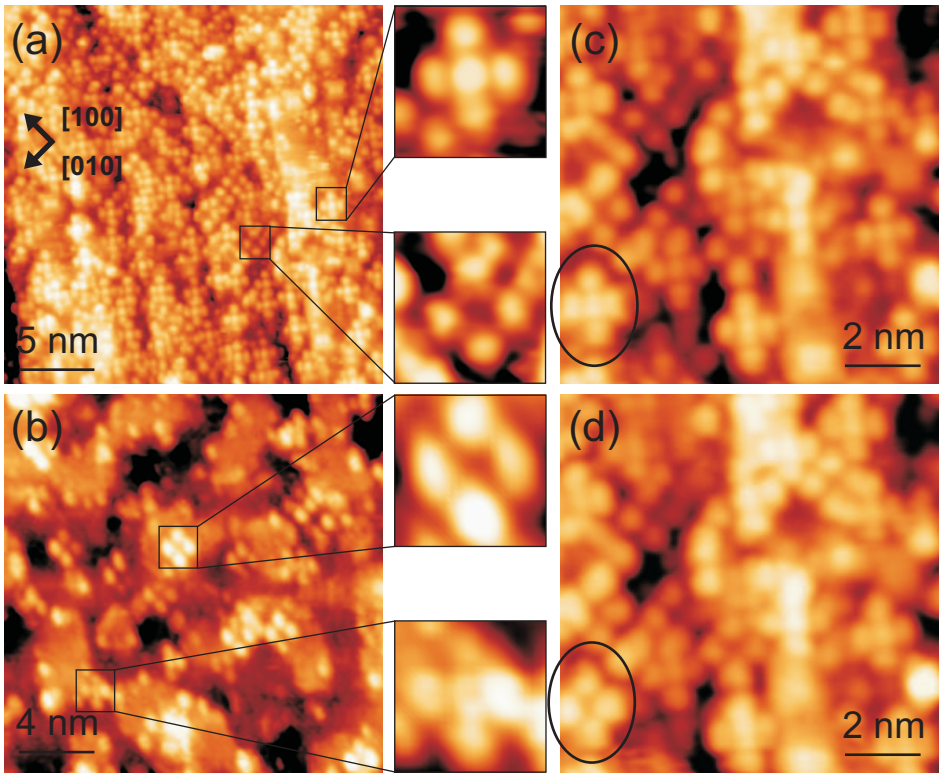

Figure 3.2: Recognition of molecular features after adsorption of MnTPPCl on smooth and rough Co substrates. (a) 0.9 ML on smooth Co film, $I = 0.12$ nA, $U = -2.3$ V, 25×25 nm^2, and two different molecular shapes: with five and four lobes. **(b)** 0.3 ML on rough Co film, $I = 0.22$ nA, $U = -1.2$ V, 20×20 nm^2, and two molecular shapes. **(c), (d)** Two consecutive STM images displaying a change of the shape of the molecule from 'five-lobe' to 'four-lobe' during scanning, 10×10 nm^2, $I = 0.12$ nA, $U = -2.4$ V (c), $U = -3.0$ V (d). The crystallographic directions of the substrate are the same in all images and are indicated by the arrows in (a).

On both types of Co substrates there are two kinds of MnTPPCl molecules noticeable in the STM images: characterized by four and by five lobes they resemble different faces of a dice (cf. zoom sections provided in Figures 3.2 (a) and (b)). The fraction of "five-lobe" molecules counted from several STM images is $\sim 77\%$ for both substrates. The difference between the two observed molecular geometries has been attributed to a change in the oxidation state of Mn from 3+ to 2+ upon adsorption on the metallic substrate [37]. Such a change suggests a dissociation of chlorine atom from the MnTPPCl molecule,

as it will be detailed in Chapter 4. Yet no conclusive evidence has been presented to unambiguously explain the effect observed in the STM, therefore we will address this issue again in the following paragraphs.

Figures 3.2 (c) and (d) exhibit two consecutive STM images taken over the same area of 0.9 ML of MnTPPCl molecules on smooth Co substrate, where one MnTPPCl molecule (marked by a black oval) changes its geometry from "five-lobe" to "four-lobe". Any tip-induced effect that might explain this transition can be excluded, as the particular molecule was the only one affected in the image and both types of molecules continue to be present in the image. Additionally, there was neither a dramatic difference in the bias voltage between the two images (-2.4 V and -3.0 V, respectively), nor in the tunneling current (0.12 nA for both), that could induce such change in the molecular appearance. We attribute, this transition to a variation in the valence of Mn ion e.g. from 2+ to 3+ oxidation state.

Assuming the removal of Cl from MnTPPCl when adsorbed on Co, the resulting molecule would exhibit an empty position in the octahedral symmetry of Mn which provides a valence to be occupied by an externally supplied ligand. Mn(II)TPP is known to have a very high affinity for an axial ligand [77, 78], therefore it is a reasonable assumption that it also reacts with the components of the residual gas in the UHV. Due to the low vacuum pressure of the order of 10^{-10} mbar in the experimental chamber, this reaction is very rare and difficult to observe. Consequent to this hypothesis, the "five-lobe" and the "four-lobe" molecular appearances are tentatively assigned to be Mn(II)TPP and Mn(III)TPPCl (or oxidized Mn(III)TPP), respectively.

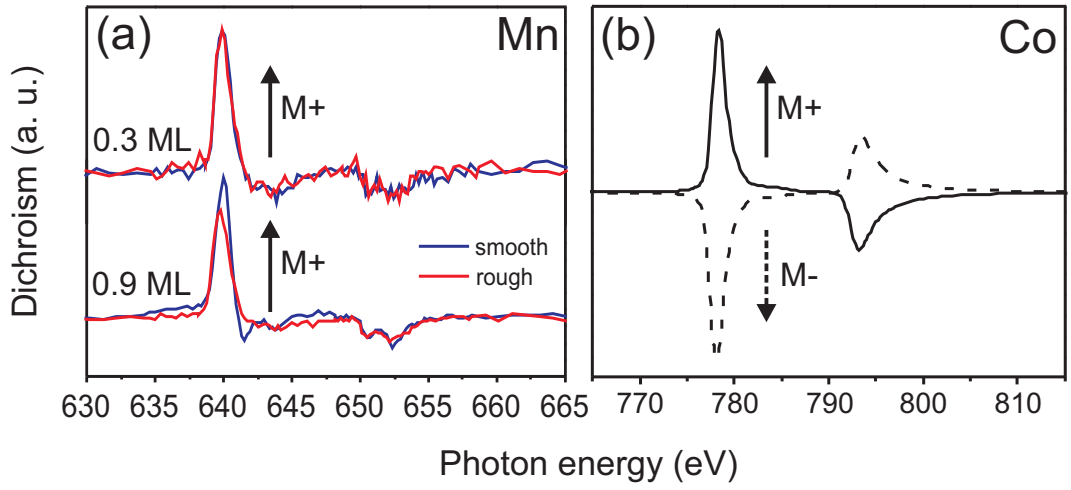

Figure 3.3: XMCD spectra of Mn and Co in the MnTPPCl/Co system. (a) MnTPPCl molecules on smooth (blue) and rough (red) Co substrates for 0.3 (top) and 0.9 (bottom) ML coverage (for easy comparison, only one direction of the Co substrate magnetization (M+) is shown) and **(b)** XMCD spectra of the Co substrate for two opposite magnetization directions: M+ and M−.

To address the question about the character of the magnetic interaction between MnTPPCl layers and the Co substrate, we have plotted Mn $L_{2,3}$ edges XMCD spectra recorded for two coverages of MnTPPCl: 0.3 ML (Figure 3.3 (a), top) and 0.9 ML (Figure 3.3 (a), bottom) on smooth (blue) and rough (red line) Co substrates. There is a clear effect of surface roughness on the XMCD signal for high coverage (0.9 ML) of MnTPPCl molecules which was neither observed nor reported earlier, while there is almost no difference observed between the XMCD signals recorded for smooth and for rough Co substrates for low molecular coverage (0.3 ML). The similar shape of the XMCD signal for 0.3 ML of MnTPPCl adsorbed on the smooth and on the rough substrate indicates that the adsorption statistics (on the step edge sites vs. terrace sites) is similar on both. This means that at the same coverage (here 0.3 ML) the number of molecules adsorbed at step edges is about equal for smooth and for rough Co films. Therefore no conclusion about the origin of the magnetic interaction can be drawn from the experiments at this coverage. At higher molecular coverage however, the surface gets progressively occupied and the adsorption site statistics may be altered by the tendency of the porphyrin to adhere to less favorable sites before nucleating a second layer. The significantly reduced (by $\sim 30\%$) XMCD signal for a close to full monolayer coverage of MnTPPCl on the rough Co substrate provides evidence that: (i) the statistics of adsorption is modified due to the high density of step edge sites present, and (ii) that the Mn coupling of MnTPPCl at the latter sites is reduced. Thus, our data supports that the dichroism, i.e. the magnetic coupling is favoured by the flat adsorption geometry of the porphyrin and is reduced by molecules taking step or kink positions at higher molecular coverage on rough substrates. This also indicates that the chemical and/or electronic interaction of the molecules differs between the step edge position and the flat adsorption on the terrace.

3.2 Theoretical calculations

The presented experimental results have been complemented by two sets of theoretical calculations: (i) cluster DFT for Mn(II)TPP and Mn(III)TPPCl and (ii) DFT+U for Mn(III)PCl with Cl atom pointing either up (towards vacuum) or down (towards the substrate). DFT cluster calculations were performed for two porphyrin configurations: with and without the axial ligand (see insets in Figure 3.4). The Co(001) surface was represented by the Co_{14} cluster. During relaxation, the atoms in the supported clusters were allowed to move in 3D space.

Insets of Figure 3.4 present the structure of the porphyrin placed above Co(001) surface, which is represented by a Co_{14} cluster. The optimal Mn-Co distances in cluster-DFT calculations are equal to 4.15 and 3.67 Å for the Cl-ligated and unligated Mn-porphyrin, respectively. Whereas the N-Co distance is computed to be 3.88 Å, the stabilization

energies for the Cl-ligated and unligated Mn-porphyrins have been determined as -0.29 and -0.33 eV, respectively. The fact that numerical models converge for both molecular configurations further supports our experimental evidence that both these forms can be present at the surface of the Co substrate. Figure 3.4 shows the spin-resolved partial

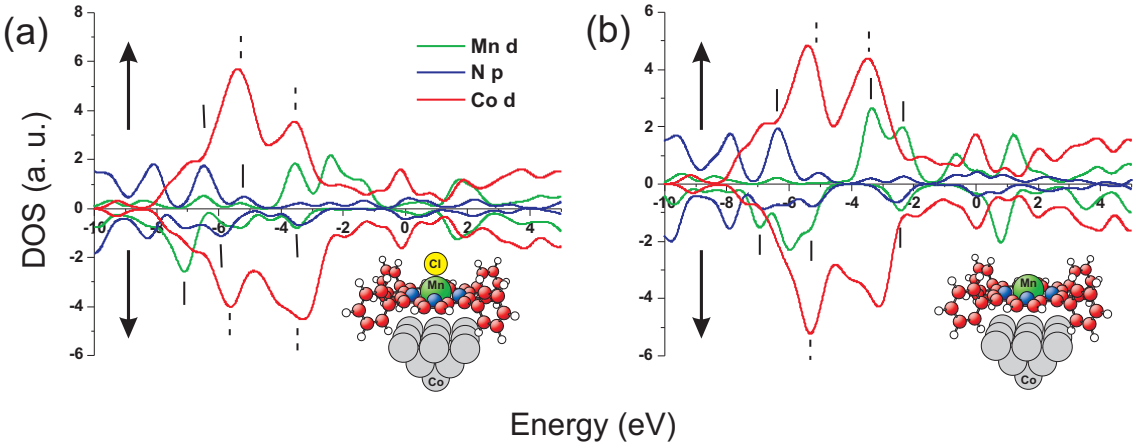

Figure 3.4: Calculated partial DOS of the Mn porphyrin with and without the axial Cl ligand. (a) With chlorine. **(b)** Without chlorine. Solid vertical bars indicate common Mn and N partial DOS peaks, and dashed vertical bars denote common N and Co partial DOS peaks. Black arrows represent spin-up and spin-down configuration. Insets display the structure of the Mn porphyrin molecule above the Co_{14} cluster with the chlorine atom pointing up (a) and without chlorine (b).

density of states (DOS) for the porphyrin with and without chlorine supported at the Co cluster ((a) and (b), respectively). Black arrows represent the respective spin-up and spin-down configurations. The hybridization of Mn and N electronic states can be realized from the coincidence of DOS peaks at the same energies for Mn 3d and N 2p states (marked by solid vertical lines in Figure 3.4). A small Co-N hybridization, however, is evidenced by the calculated partial DOS (see the dotted vertical lines), which suggests that there is a weak electronic interaction between the N centers of the porphyrin and the Co centers of the substrate as it was also shown by Wende *et al.* for the coupling of Fe(II)OEP to Co(001) [15].

DFT+U calculations were performed to investigate the chemical and magnetic interaction of a MnPCl molecule with a ferromagnetic Co surface. In contrast to the cluster calculations, the molecule and three atomic Co layers were represented within a large supercell and periodic boundary conditions were applied to capture the periodicity of the surface. Also, the four phenyl rings have been removed (and replaced with hydrogens) in order to reduce the computational effort; i.e. the DFT+U simulation was performed for a MnPCl molecule. In the simulations, the metallic surface was modeled through three atomic layers of Co (adopting the fcc Co lattice parameter of 3.61 Å). Furthermore, a full 3D geometric optimizations of the porphyrin molecule and its position on the surface

was performed. To reduce the computational effort, the bottom two layers of Co atoms were fixed in the simulations. Through test calculations, it was verified that this is indeed a good approximation; complete relaxation of all atomic distances revealed that the molecule-surface distances (and consequently, interactions) did not change, but a small relaxation of the top to second Co layer occurred. The geometric relaxation of the MnPCl on the surface was performed for two different configurations: in the first case, (i) the Cl atom is on top of the molecule oriented away from the surface, whereas in the second case (ii) the Cl atom is between the porphyrin ring and the surface. Assuming that the coupling mechanism of Mn(II)TPP is similar to Fe(II)OEP, DFT+U calculations have been performed on an intact Mn(III)PCl molecule to complement the earlier work. The focus of the calculations was the chemical and magnetic interactions of the Mn(III)PCl with the Co surface. As expected, it has been found that the orientation of the Cl atom largely influences these interactions. Considering first the situation (i), a stable molecular configuration has been obtained. In this configuration the central Mn atom has moved (by 0.4 Å) out of the porphyrin plane due to the bonding to the chlorine. The distance of the porphyrin ring to the Co substrate is 3.49 Å, typical for physisorbed porphyrins. The computed molecular spin is $S \approx 2$, i.e. practically the same as the one expected for a free MnPCl molecule. The coupling of the molecule's spin to that of the surface Co atoms is found to be weak, in the order of less than 5% of the MnP/Co interaction which calculates to 34 meV [79] yet a parallel (ferromagnetic) coupling is preferred. In Figure 3.5 we show the DFT+U computed partial DOS of this system. We use here the experience, which has been gained in the past when using atom-resolved DOS plots for composite materials [79, 80]. The occurrence of narrow partial DOS peaks at the same energy exemplifies the occurrence of, in this case, bonding of Mn and Cl orbitals. In Figure 3.5 green vertical lines indicate the coinciding Cl and Mn orbitals, and blue vertical lines indicate the positions of the coinciding N and Co orbitals. Therefore, it is apparent that the Cl atom binds to Mn, furthermore, Mn is bound to the nitrogen through the chemical structure of the porphyrin and N atoms exhibit bonding to the Co substrate. This observation illustrates the role of the nitrogen atoms in mediating an indirect magnetic coupling of the Mn and Co atoms.

The situation (ii) in which the Cl atom is located between the Mn and the Co surface gives rise to a rather different chemical bonding and consequently, magnetic interaction. This geometry is unfavorable for the bonding of monovalent chlorine, which does not sustain two bonds, one to the Mn and one to Co atom. It has been found in the structural relaxations that the Cl atom moves away from the Mn and closer to a surface Co atom, i.e. the Mn-Cl bonding weakens in favor of a stronger Cl-Co bond. This shift of the chemical bonding is reflected in the molecule's spin which is increased to $S \approx 5/2$, which is in fact the high-spin value expected for a free MnP molecule [79]. Also, the magnetic coupling of the molecule's spin to the surface has now become weakly antiferromagnetic.

This finding suggests that when the Cl binds to a Co atom, a MnP molecule might be liberated and could interact ferromagnetically with the Co substrate at another location. Notably, this is supported by the experimental observation of the Cl-dissociation as reported earlier in this chapter.

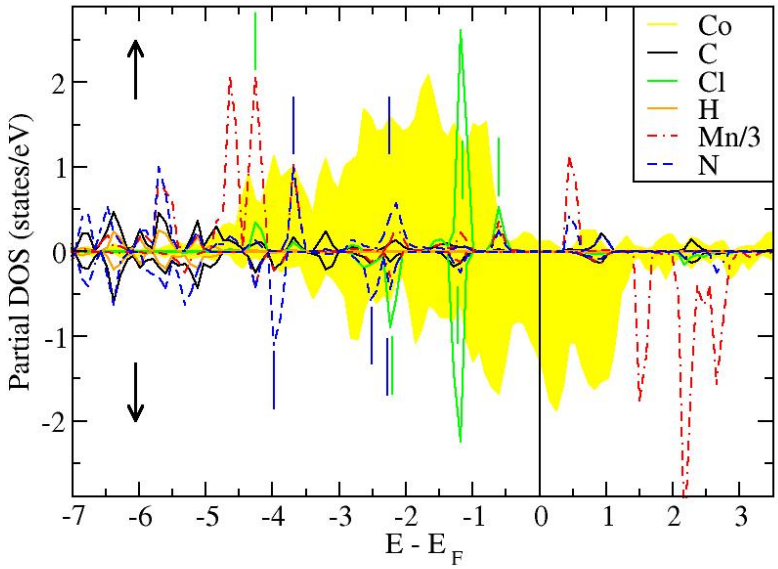

Figure 3.5: Calculated spin-polarized partial DOS for a MnPCl molecule on a Co substrate with the Cl atom oriented away from the surface. Joint partial DOS peaks illustrate that both chlorine and nitrogen bond to Mn. The blue vertical bars illustrate a bonding of the molecule's nitrogens to Co surface atoms and the green vertical bars a bonding between Mn and Cl within the molecule. The Fermi level (E_F) is at 0 eV and the spin-up, respectively, spin-down partial DOS panels are indicated by the arrows.

Overall, the presented theoretical calculations based on cluster DFT and DFT+U complemented the experimental XMCD and STM data. Specifically, we observe a pronounced Mn-XMCD signal (both on smooth and rough Co) at $\sim$ 639.9 eV and a shoulder at $\sim$ 641.2 eV. We assign the former (peak) structure to the Mn^{2+} species i.e. to MnTPP formed by removal of Cl from MnTPPCl adsorbing onto the substrate surface with the Cl-atom pointing towards Co as predicted by the DFT+U calculations. Consistently, we assign the second (shoulder) structure to the Mn^{3+} species i.e. to MnTPPCl adsorbing with Cl pointing up. On the basis of the statistics of the molecular appearance in our STM data we assign the former (peak) structure to the "five-lobe" molecular feature, and the latter (shoulder) structure to the "four-lobe" feature. Both species are ferromagnetically coupled to Co as revealed by the XMCD data which is consistent with the presented calculations.

3.3 Conclusions

The presented study provides conclusive evidence on the basis of XMCD, STM and first principles cluster DFT and DFT+U calculations towards the identification of the molecular species involved in the magnetic coupling observed after deposition of MnTPPCl molecules to pre-magnetized smooth and rough Co thin film substrates. STM images confirm the flat-lying adsorption geometry of Mn porphyrin molecules on the surface. DFT calculations confirm the coexistence of ferromagnetically coupled Mn-porphyrins, with and without Cl, and validate the assignment of the species on the basis of the experimental results. Specifically, the geometry with the Cl atom located between Mn and the Co surface is not favourable in the calculations while the geometry with the Cl oriented away from the surface is chemically more stable.

A second conclusion results from the XMCD signal at the Mn $L_{2,3}$-edge which was found to be higher on smooth than on rough Co films at high molecular coverage. This observation supports the indirect-coupling mechanism in agreement with the presented calculations. Specifically, the overlap of the porphyrin N p-orbitals with the Co d-orbitals is observed to be strengthened as the Mn atom is moved out of the porphyrin plane.

CHAPTER 4

Substrate induced magnetic and structural ordering of a molecular monolayer[1]

We have seen in the previous chapter, that MnTPPCl molecules couple ferromagnetically to the Co substrate by an indirect exchange interaction. It has also been demonstrated that the strong molecule-substrate interaction leads to a partial molecular decomposition. In this chapter we will compare the magnetic and structural behaviour of MnTPPCl on two substrates: atomically clean Co (Co(001)) and oxygen-covered Co (O/Co(001)). The results show that a chemical passivation of the substrate leads to interesting new effects involving both: magnetic and chemical interactions.

The preparation procedures for Co(001) and for O/Co(001) substrates are described in Chapter 2. The magnetization of MnTPPCl on Co(001) and on O/Co(001) was studied by XMCD [58] at the L_2 and L_3 absorption edges for both Co and Mn species separately. The oxidation state of the central metal atom of the molecular film as well as the chemical bonding to the substrate was studied by XAS and XPS. The structure of the substrate and the MnTPPCl adlayer for the two systems were studied by STM. Complementary structural information was obtained from LEED experiments.

[1] The results of this chapter were published in *Journal of Physical Chemistry Letters* **1**, 1408 (2010)

4.1 Magnetic properties and chemical identification of the adsorbates

A monolayer of MnTPPCl molecules adsorbed on Co(001) and on O/Co(001) substrates gives an XMCD signal in the Mn photon energy, indicating a magnetic moment present in the Mn species (Figure 4.1). The XMCD data in Figure 4.1 (a)-(d) show two X-ray absorption spectra recorded with radiation of opposite circular polarization (circ+ and circ-, dashed and solid lines, respectively) and their difference (curve with a coloured area).

The relative signs of the Mn and Co XMCD spectra (e.g. at L_2 and L_3 edges) signify a ferromagnetic (FM) coupling mechanism of MnTPPCl on Co(001) and an antiferromagnetic (AFM) coupling mechanism on O/Co(001). It was manifested in both magnetization directions of the underlying Co layer (only one direction is presented). The following relevant coupling mechanisms have been proposed: (i) an indirect FM coupling via N atoms of the molecule on Co(001) and (ii) a superexchange mechanism via the oxygen atoms for the AFM coupling on O/Co(001) substrate, as derived from DFT+U calculations [15, 23, 81]. Notably, neither the exact atomic geometry of the substrate nor the chemical/physical bonding of the adsorbed magnetic molecules, which is a crucial determinant for the system-specific coupling mechanisms between molecular spin systems and magnetic substrates, have been addressed so far in detail in the previous works. In the following, we discuss the magnetic coupling between the molecule and both substrates.

As a first observation, it is important to note the shift of the peak position of Mn absorption spectra between $\sim$ 639.9 eV on Co(001) substrate and $\sim$ 641.2 eV on O/Co(001) (see the dotted lines in Figure 4.1 (b) and (d)). Such a shift in XAS is usually associated with a change of the oxidation state of the studied material. To answer the question about the exact chemical species adsorbed on the Co substrates, we have recorded additional XAS spectra for two references: MnO and Mn_2O_3, with the Mn oxidation states 2+ and 3+, respectively to compare with the MnTPPCl data (Figure 4.1 (e)). It is evident, that for a MnTPPCl/Co(001) system, manganese exists mostly in 2+ and for MnTPPCl/O/Co(001) in 3+ oxidation state. The dominance of Mn^{2+} in the MnTPPCl adsorbed on the Co(001) substrate indicates a partial decomposition of Mn(III)TPPCl on the surface, that is, by dissociation of Cl, as it has been proposed in Chapter 3. This dissociation would correspondingly change the spin magnetic moment of Mn from 4.90 to 5.92 μ_B (if Mn-porphyrin is assumed to remain on the surface in the high-spin configuration) [23, 82]. FM exchange coupling is rather associated with the Co-Mn bonding configuration than with the Co-Cl-Mn bonding configuration. In the latter case, AFM contributions are expected in the XMCD spectra because of the possibility of superexchange interaction via the Cl atoms, as it has been predicted by the DFT+U

calculations presented in Chapter 3. Such a signal is not observed in our experiments. On the oxygen-covered substrate, on the contrary, the predominance of Mn^{3+} signal at ~ 641.20 eV (Figure 4.1 (e)) in the Mn L_3 XAS suggests that the molecules stay intact during sublimation and also upon the adsorption process. The issue of the exact chemical species adsorbed on the two different substrates will be raised again in the following section and explained in detail on the basis of STM and XPS results.

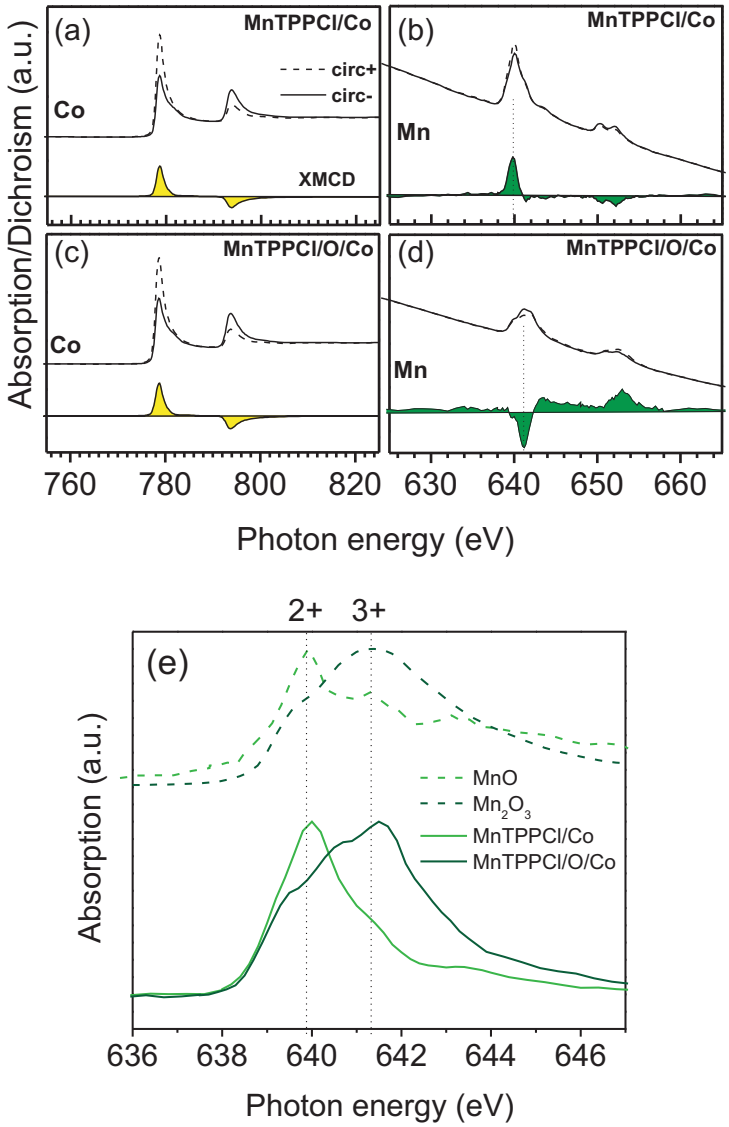

Figure 4.1: XAS and XMCD spectra acquired on (a, b) Co(001) and (c, d) O/Co(001) substrates after deposition of MnTPPCl molecules. Co and Mn XAS L-edges for opposite helicities of incoming X-rays (dashed – circ+, solid – circ-) and their respective dichroic signals (curves with coloured areas). Note that Mn-XMCD signals at the L_3 edge on Co(001) and O/Co(001) are at (b) ~ 639.90 eV and (d) ~ 641.20 eV photon energy (marked by dotted black lines) reflecting the presence of Mn^{2+} and Mn^{3+} species on the respective substrate. **(e)** Zoom in of the Mn L_3-edge XA spectra (solid lines) compared with two reference samples: MnO and Mn_2O_3 (dashed lines) signifying different oxidation states of MnTPPCl on Co(001) and on O/Co(001).

The second important observation at the Mn XAS signal is the spectral shape of the L_3 peak. While the MnTPP/Co(001) reveals a narrow L_3 edge, the MnTPPCl/O/Co(001) displays a very broad feature. Having in mind that XAS reveals the density of empty (in this case) 3d states, it is clear that Mn^{3+} species (having six unoccupied states) will reveal more spectral features than the Mn^{2+} species (five unoccupied states).

Information about the relative spin configuration of the Mn ion can be deduced from the magnitude of the Mn dichroic signal compared for molecules adsorbed on Co and on O/Co. Figure 4.2 (a) presents that the magnitude of the circular dichroism is higher on O/Co (green) that on Co (orange), indicating that more spins contribute to the Mn magnetic moment in the Mn^{3+} species. Assuming a high-spin configuration, Mn^{3+} with four electrons in 3d orbitals, can have a spin of $S_{Mn} = 2$, whereas Mn^{2+}, $S_{Mn} = 5/2$. This assumption is, however, in disagreement with the experimental data presented in Figure 4.2. We therefore postulate, that the Mn in the MnTPP molecule changes its spin state from high-spin (HS, $S_{Mn} = 5/2$) in the bulk phase [83, 84] to intermediate- (IS) or low-spin (LS) ($S_{Mn} = 3/2$ or $S_{Mn} = 1/2$, respectively), when adsorbed on the Co surface. The electron configuration of Mn in case of MnTPPCl adsorption on O/Co remains HS ($S_{Mn} = 2$), like in a Mn(III)TPPCl molecular crystal [71].

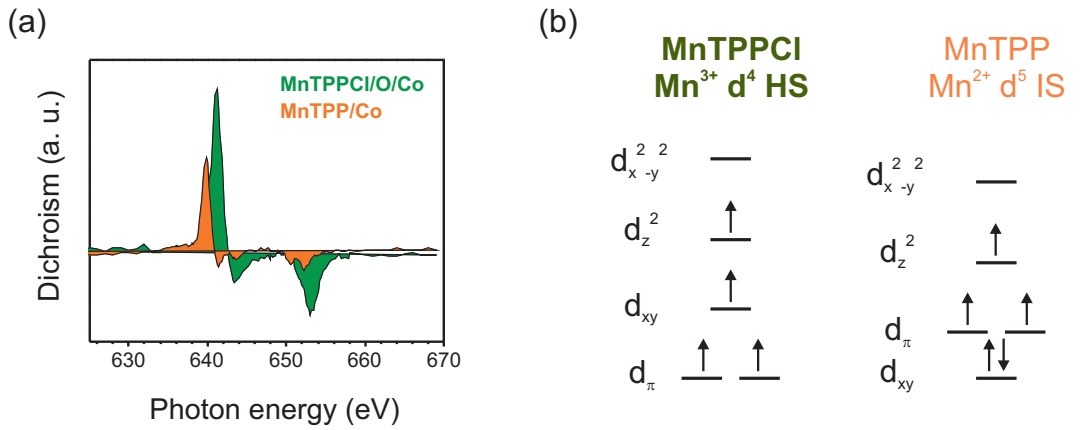

Figure 4.2: Spin configurations of Mn in Mn(II)TPP and Mn(III)TPPCl. **(a)** Mn XMCD spectra of MnTPPCl on Co and O/Co substrates. Height of the dichroism indicates the number of unpaired spins. **(b)** Tentative electron occupancy of the Mn 3d levels in the HS Mn(III)TPPCl and IS Mn(II)TPP.

The identification of IS (or LS) configuration of Mn upon adsorption of MnTPP on Co is an effect which has not been discussed before. DFT+U calculations performed for a similar system [79] predict that a Mn-porphine (MnP, without phenyl rings), initially with $S_{Mn} = 5/2$, donates one electron to the Co substrate upon adsorption, and consequently becomes $S_{Mn} = 2$. On the other hand, DFT simulations of a free MnP molecule show that in the ground state the spin of Mn equals 3/2 [85]. These discrepancies within theoretical calculations prove that the system under study is indeed very complicated

and its behaviour cannot be easily modeled. Depending on the computational routine (DFT+U or DFT) various results are obtained [79, 85]. Because the spin of Mn ion in the molecule depends strongly on the ligand field, different electron configurations will be computed for a square planar, square pyramidal or octahedral crystal field. Additionally, important questions arise, whether the substrate should be treated as a ligand, or whether Mn stays in plane of the macrocycle. The disagreement between theory [79] and the here described experiment can also stem from simplifications used in the calculations, which are necessary for reducing the computational time. The removal of phenyl rings performed in the simulations can result in a different than in experiment molecule-substrate distance and hence – interaction. Furthermore, it has been shown [24] that including, the here [79] neglected, long-range van der Waals interactions improves the agreement between the experiment and calculations. In conclusion, as mentioned in the Introduction, the experimental results in this case are more trustworthy than calculations, therefore we postulate an IS configuration of Mn ($S_{Mn} = 3/2$) in Mn(II)TPP adsorbed on Co(001) and HS ($S_{Mn} = 2$) for Mn(III)TPPCl/O/Co, as presented in Figure 4.2 (b). It is important to note, that for MnTPP a square planar geometry is assumed and for MnTPPCl – a square pyramidal geometry.

4.2 Structure and morphology

Toward a conclusion on the magnetic coupling mechanisms, this section focuses on the correlation of adsorbate/substrate chemical structure and bonding with the magnetic interaction determined from XMCD. The STM data indeed revealed remarkable differences in the step arrangement between the two substrates. On the O/Co(001) (Figure 4.3 (a)), steps are well aligned with the [100] and [010] directions forming a rectangular pattern, whereas growth of Co(001) (Figure 4.3 (d)) results in rounded islands and step edges with little or no correlation to the crystallographic directions. Such a change in the step arrangement of Co suggest a formation of an oxide on the surface, as previously observed by STM [86]. The LEED pattern of the O/Co(001) substrate (inset in Figure 4.3 (a)) shows additional points compared to the LEED of metallic Co(001) (see inset of Figure 4.3 (d)), indicating a c(2 x 2) oxygen superstructure as reported in the literature [51].

Notably in our STM results, also the molecular assembly of MnTPPCl on c(2 x 2)-O/Co(001) (Figure 4.3 (b)) was found to differ clearly from the assembly on atomically clean Co(001) substrate (Figure 4.3 (e)). Whereas MnTPPCl molecules evaporated onto Co(001) were adsorbed in a random fashion, on O/Co(001), self-assembled and well-ordered molecular domains were formed. Two mirror domains, at the angle of 22° with respect to each other, can be identified on the STM image (Figure 4.3 (b)), that is, a 2D chirality. The formation of such self-assembled 2D chiral domains of nonchiral MnTPPCl

molecules is well known in the context of surface molecular assembly; it has been observed for the assembly of nonchiral cobalt(II)tetraphenylporphyrin (CoTPP) on Au(111) [87], where a balance of "molecule-molecule" and "molecule-substrate" interactions played the decisive role in determining the final surface configuration [88–91].

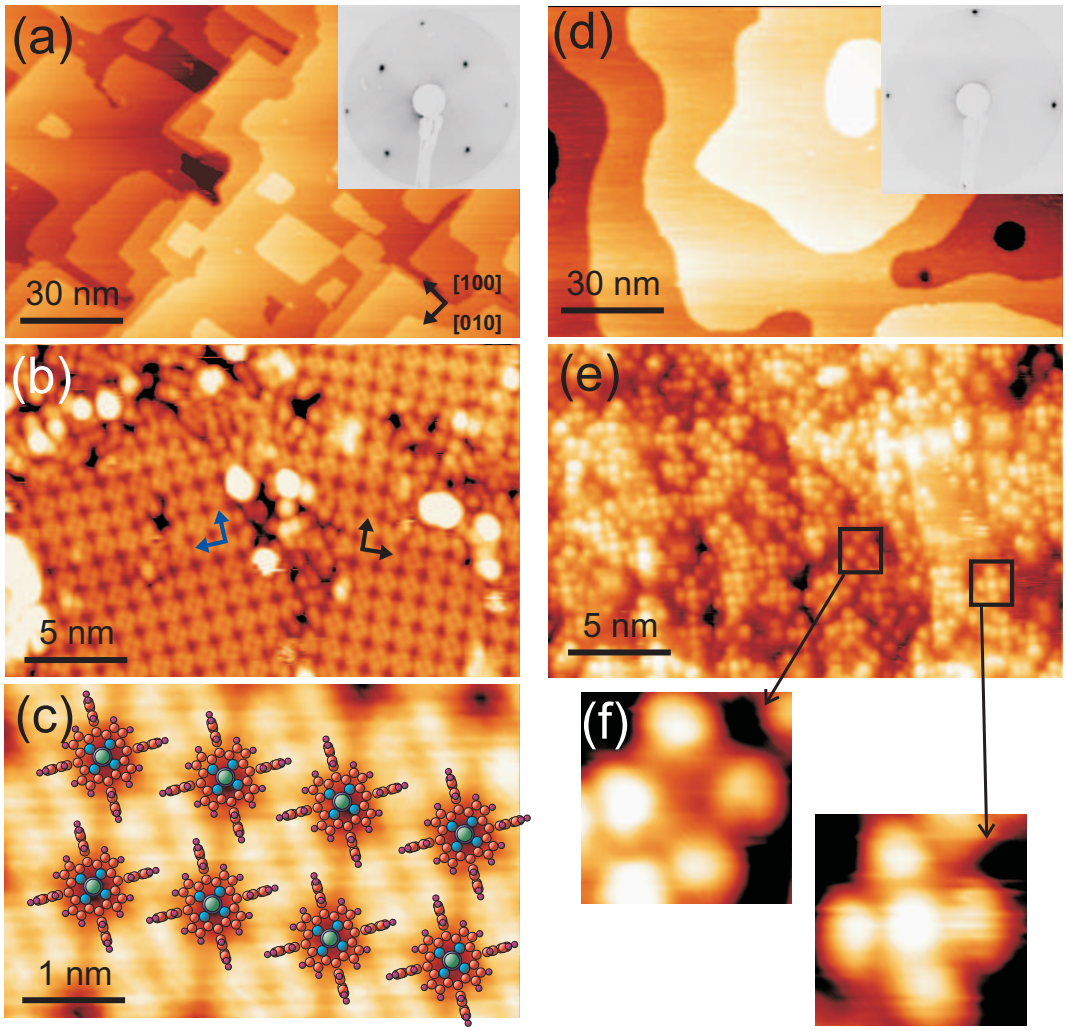

Figure 4.3: STM images of MnTPPCl on cobalt substrates. **(a, b)** oxidized Co without and with MnTPPCl molecules, respectively. The black arrows in (a) represent in-plane crystallographic directions that apply to all STM images; the blue and black arrows in (b) indicate two mirror domains also observed in LEED. **(d, e)** Co(001) without and with the molecules, respectively. **(c)** Zoom into self-assembled molecules on O/Co(001) and **(f)** into two types of molecules present on Co(001). Insets: LEED patterns taken at 53.2 eV on (a) O/Co(001) and (d) Co(001). Acquisition parameters for the STM images (I, V): (a) 0.06 nA, 1.0 V; (b) 0.08 nA, -3.0 V; (d) -0.13 nA, -0.6 V and (e) 0.12 nA, -2.3 V.

For molecules with C4 symmetry, for example, MnTPPCl on a substrate with C4 symmetry, two mirror domains of assembly are expected to exist, which is consistently observed in the LEED and STM data for MnTPPCl molecules on the O/Co(001) substrate. The observed molecular assembly corresponds well with previous results on the self-assembly

of porphyrins on substrates with higher or lower reactivity [32, 88–90, 92].

The porphyrin/substrate interaction, which is an important factor influencing the self-assembly, as well as the magnetic coupling to the substrate, shall here first be discussed in more general physicochemical terms. It is the balance of molecule/substrate and intermolecular interactions together with the corrugation of the surface interaction potential that influences the diffusion and subsequently determines the self-assembly at a given thermal energy (k_BT) [32, 69, 87–94]. In the specific case of porphyrin adsorption, stronger interaction has been observed on metallic substrates than on ultrathin insulators [32], the latter substrate possibly providing an analogue to the O/Co(001) surface.

Therefore, the disordered arrangement of MnTPPCl on Co(001) provides evidence of a considerable potential diffusion barrier that prevents the self-assembly during and after the deposition process. Specific to MnTPPCl is the broken symmetry caused by the axial Cl-Mn bond, which also introduces an electric dipole. The self-assembly of dipole containing molecules with axial symmetry on more or less reactive substrates has been studied for the case of subphthalocyaninato chloride (SubPcCl) [69, 93, 94]. For the SubPcCl, the issues of molecular orientation and self-assembly have been identified by a combined STM and XPS study, which revealed the presence of a chemical bond between the molecule and the Ag substrate, not observed in the case of the Cu substrate. On vacancy islands in an ionic crystal substrate, the same molecules are oriented toward the polar pockets fitting the negative Cl polarity best [32]. These processes have been related to the Coulomb potential affecting both: the molecular orientation and the assembly. MnTPPCl also contains an electric dipole ($Mn^{\delta+}$-$Cl^{\delta-}$), which by itself is affected by the electronic interaction with the substrate and contributes to a "dipole-dipole" interaction in the specific case of the more chemically inert $Co^{\delta+}$-$O^{\delta-}$ surface dipole layer, therefore enhancing the formation of self-assembled molecular domains of MnTPPCl on the O/Co(001) substrate.

The assembly of molecules on O/Co(001) is further confirmed by the characteristic LEED pattern shown in Figure 4.4 (a). In contrast, no molecular LEED pattern could be observed for 2D arrangement of molecules on Co(001) substrate. To draw conclusions on the recorded LEED pattern, we performed a simulation of the molecular arrangement with respect to O atoms of the reconstruction (compare Figure 4.4 (a), (b) and (c)). The mirror domains are rotated by $\pm 11°$ with respect to the mirror planes, which are in the [110] and [1-10] directions. By comparison of the LEED data with the simulated pattern (Figure 4.4 (a) and (b)), the molecular lattice with respect to the reported c(2 x 2)-O superstructure can be expressed in a matrix notation as:

$$M = \begin{pmatrix} 2.5 & \pm 0.5 \\ \mp 0.5 & 2.5 \end{pmatrix}.$$

The matrix indicates the relative position of MnTPPCl molecules with respect to the surface O atoms, as depicted in Figure 4.4 (c). The mirror domains are marked by black and blue arrows in the STM image (Figure 4.3 (b)) and in the simulated LEED pattern (Figure 4.4 (b)). The molecular lattice constant derived from the LEED simulation gives a value of ~ 1.27 nm, which is in good agreement with the Mn-Mn spacing measured in the STM image: ~ 1.20 nm (compare Figure 4.3 (c) and Figure 4.4 (c)). One can further note that this commensurate configuration allows every molecule to match identical sites on the surface: with phenyl rings and Mn ions aligned on top of oxygen atoms of the reconstruction, as discussed below.

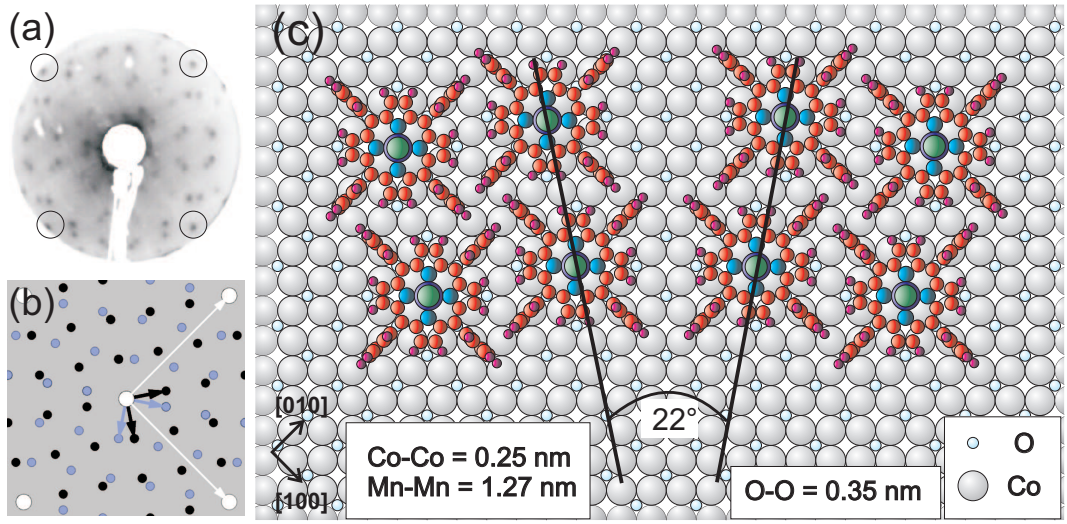

Figure 4.4: MnTPPCl assembly on O/Co(001). (a) LEED pattern of 1 ML MnTPPCl on O/Co(001) recorded at ~ 28.4 eV; circles indicate c (2×2)-O reconstruction; **(b)** simulated LEED pattern for MnTPPCl on O/Co(001) with respect to O reconstruction (white spots); two mirror domains were observed (black and blue arrows). **(c)** A tentative model of molecular arrangement on O/Co(001) surface derived from the LEED simulation (molecular atoms: red – C, blue – Mn, green – Cl, cyan – N, violet – H).

Notably, we have also observed the self-assembly of MnTPPCl molecules on Ag(111) surface, and the size of the molecular unit cell for MnTPPCl/Ag(111) was found to be ~ 1.24 nm, which is close to the size of the unit cell of MnTPPCl on O/Co. Interestingly, the size of the identified molecular unit cell in self-assembled domains for similar metalloporphyrin molecules was found to be larger (e.g., for CoTPP/Ag(111): ~ 1.40 nm [87, 92]) than that for both MnTPPCl/O/Co(001) or MnTPPCl/Ag(111) systems.

One reason for such differences in the unit cells can lie in the molecular arrangement; in particular, the orientation of the phenyl rings (planar vs. upright) and the competition of intermolecular interaction (mostly van der Waals interaction and dipole/dipole interaction) versus molecule/substrate interaction can lead to different packing densities of similar molecules. Furthermore, the typical molecule/substrate interaction as discussed above can also play an important role in the observed high surface molecular packing.

Not only does the assembly of molecules look different on the two different substrates but also the appearance of the molecule itself is an important feature here. On the O/Co(001) (Figure 4.3 (b)), all molecules look identical and it is obscure where a single molecule has its lobes or how it is adsorbed on the surface. A zoom-in into molecular lattice containing a defect site presented in Figure 4.5 can serve as guidance in recognizing the adsorption geometry. The shape of the vacancy exactly matches the molecular structure and provides an unambiguous proof of the adsorption geometry with a depression as a center of a molecule ("four-lobes" geometry).

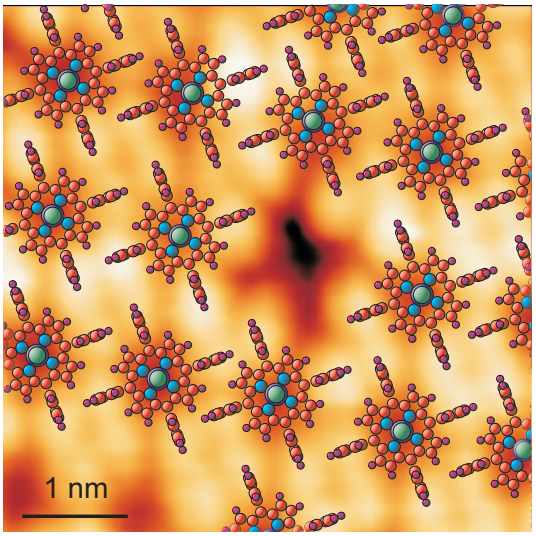

Figure 4.5: STM of MnTPPCl/O/Co(001) - assignment of molecular lobes. The way how the molecular lattice is terminated at grain boundaries and defects, e.g. vacancies, allows an unambiguous assignment of the observed depressions (dark spots) to the centers of MnTPPCl molecules.

In contrast to the uniform molecular appearance on O/Co(001), on metallic Co(001) (Figure 4.3 (d)), one can clearly distinguish two different molecular geometries: with "four-lobes" and with "five-lobes" (protrusion in the center; see Figure 4.3 (f)). This issue, raised already in the previous chapter, might point to some ambiguity in the determination of the chemical composition of the adsorbate. Possible interpretations of the two appearances visible in the STM images are: (i) different orientation of the Cl, either pointing down (toward the substrate) or up (toward vacuum), (ii) removal of Cl in some molecules, either during the evaporation process or (iii) due to a chemical reaction upon adsorption onto the Co(001) substrate.

Possibility (i) has been already clarified in the previous chapter, resulting in a conclusion that only Cl-up configuration can be found on Co surface. Possibilities (ii) and (iii) lead us back to the issue raised in the former section, namely the identification of the exact chemical species adsorbed on the surface. To rule out molecular decomposition occurring during the evaporation process (ii), we have recorded UV-Vis spectra (Figure 4.6 (a))

for MnTPPCl molecules in dimethylsulfoxide (DMSO) at three different stages of the experiment: (a) as received from the manufacturer, (b) as residual left in the evaporator after the XMCD measurements, and (c) as separately sublimed. All UV-Vis spectra show the same spectral features, which provides significant evidence against molecular decomposition of MnTPPCl during the evaporation.

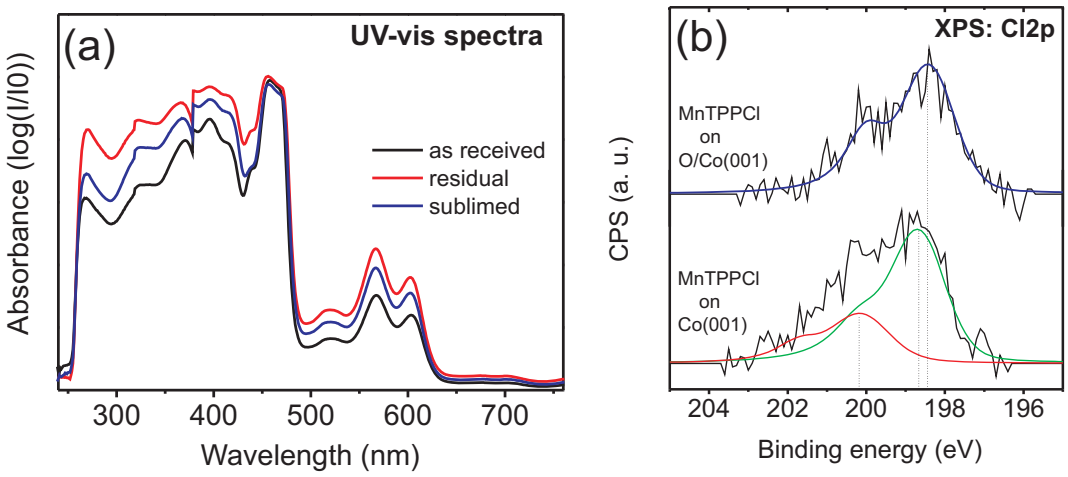

Figure 4.6: Cl dissociation upon adsorption on Co(001). (a) UV-Vis spectra of MnTPPCl molecules in three stages of the experiment: fresh from supplier (black), residual from the evaporator (red) and separately sublimed (blue) all showing the same spectral features. **(b)** Cl2p XP spectra of MnTPPCl on O/Co(001) (top) and on Co(001) (bottom) revealing different spectral widths: on O/Co(001) only one doublet (blue line) constitutes the spectrum, while on Co(001), two (red and green curves) contributions could be fit.

In line with our previously discussed XAS results (see former section) the change of the Mn oxidation state from 3+ to 2+, upon adsorption of MnTPPCl onto the Co(001) substrate, is attributed to the removal of Cl from the molecule. Considering the chemical reactivity of an atomically clean bare metal surface, the probability of such decomposition occurring on the Co(001) substrate should be much higher than that on the O/Co(001). To confirm the partial-Cl-loss-issue upon adsorption (iii) we have performed Cl2p XPS measurements on the two substrates. The XPS data (Figure 4.6 (b)) indicate the presence of chlorine on both substrates, which in a first glance seems to contradict the removal of Cl. At this point, it is important to note, that a Cl2p peak is a doublet in nature due to a spin-orbit interaction [50]. A closer look at the spectra reveals that the Cl2p peak in MnTPPCl/Co system exhibits a broader shape than the one in MnTPPCl/O/Co. In line with the previously reported data on Cl2p XPS binding energy [95], the principal peak observed on both Co(001) and O/Co(001) substrates at $\sim$ 198.5 eV ($2p_{3/2}$, blue and green fits in Figure 4.6 (b)) can be related to a $Cl^{\delta-}$ ion. Indeed, an intact molecule, contains a dipole moment with a partial negative charge on Cl, as discussed before. The peak observed for Co at $\sim$ 200 eV, is tentatively assigned as to

come from the Cl species physisorbed on the Co substrate. Because of the considerable reactivity of atomically clean Co(001), which may play a decisive role in the catalysis of this process, the Cl remains bound to the substrate even after dissociation from the molecule. This interpretation is supported by the DFT+U calculations presented in Chapter 3. Considering the statistics, where $\sim 77\%$ of molecules were identified to contain Mn in 2+ oxidation state, the amount of physisorbed Cl should be substantially higher than presented in Figure 4.6 (b). It has been shown that on metallic substrates, Cl can form an ionic bond with the metal atoms, leading to creation of a $Cl^{\delta -}$ ion [96, 97]. Therefore we assign the $Cl2p_{3/2}$ peak at ~ 198.5 eV on the Co substrate as containing contributions from both Cl ions: from the intact molecule and from the chemisorbed Cl on Co.

The uniform appearance of MnTPPCl on O/Co(001) substrate in the STM suggests unidirectional molecular orientation within the regular 2D domains formed by the self-assembly (Figure 4.3 (b) and (c)). The observation of an AFM exchange coupling in this case suggests the following electronic configuration: $Co^{\delta+}$-$O^{\delta-}$-$Mn^{\delta+}$-$Cl^{\delta-}$. This assignment is supported by the expectation of Cl not effectively binding to oxygen and is also in agreement with the superexchange coupling (Co-O-Mn) mechanism. Furthermore, the appearance of a single Cl $2p_{3/2}$ XPS peak at ~ 198.5 eV on O/Co(001) suggests that the Cl atoms are not directly bound to O atoms: in that case, one would expect a Cl $2p_{3/2}$ XPS peak at $\geqslant 200.0$ eV [98], which is not observed in our spectra. Therefore, our XPS and XMCD data on MnTPPCl provide support for the assigned FM (via N atoms of the porphyrin ring) and AFM (via O atoms) exchange coupling mechanisms with the Co(001) and O/Co(001) substrates, respectively.

4.3 Conclusions

Molecular assembly and magnetic ordering of MnTPPCl molecules have been studied upon deposition on Co(001) and O/Co(001). It was found that MnTPPCl molecules couple ferromagnetically to Co(001) but antiferromagnetically to O/Co(001) substrate. Our STM observations, in conjunction with the XMCD spectra and XPS data, reveal important issues compared to previous work: on the Co(001) substrate, molecules appear in two different forms and are randomly distributed across the surface. In contrast, on O/Co(001), molecules appear indistinguishable, which suggests unidirectional orientation in the self-assembled 2D domains. A significant fraction of molecules is characterized by the Mn^{2+} oxidation state after adsorption on Co(001), whereas Mn^{3+} is found almost exclusively on the O/Co(001) substrate. Hence, also in combination with UV-Vis characterization of the sublimed compound, these data indicate a partial decomposition of MnTPPCl by removal of Cl upon adsorption on the metallic Co surface, whereas on O/Co(001), the uniform appearance and oxidation state provide concerted and hitherto

significant evidence against such a molecular decomposition. Surprisingly, the molecules show a magnetic coupling to the substrate on both, the magnetic (Co(001)) layer, and the oxygen adlayer (O/Co(001)). This is despite the characteristically different adsorbate-substrate interaction of the different electronic configuration of the central metal ion of the molecules in the studied cases.

By comparing the magnitude of the Mn dichroic signal for the two systems, we have been able to identify the spin state of Mn, which is usually not possible by using sum-rules [66]. It has been found, that MnTPPCl/O/Co contains Mn in high-spin ($S_{Mn} = 2$) and MnTPP/Co – intermediate-spin ($S_{Mn} = 3/2$) configuration. Thus, upon adsorption onto the metallic substrate, MnTPPCl undergoes two processes: dissociation of Cl and change of the electron configuration from HS to IS.

Moreover, the self-assembly of magnetic molecules on the oxygen-covered ferromagnetic substrate provides a possible route toward uniform spintronic layers. Notably, the spectromicroscopy correlation approach, here involving XMCD, XPS, and STM, demonstrates its strengths to identify the mechanisms involved in organic spintronic interfaces: spectromicroscopy correlation, in combination with different adatom layer species (S, F, Cl, as known from bulk AFM materials), and magnetic molecules is expected to provide a toolbox toward the engineering of well-defined single spin systems to be addressed individually, for example, by spin-polarized STM.

CHAPTER 5

Designed change of the spin-state on the surface: switching with NO

In the previous chapter we have reported on, among other things, the spin-switching of the Mn-species from HS to IS upon adsorption on the metallic surface. Such a switching event is of a considerable interest due to the possibility of designing spintronic interfaces with tunable magnetization. However, this feature is a rather "passive" property of the interface itself and cannot be deliberately modified "from outside". The goal of the experiment described in this chapter is to intentionally manipulate the spin of a Mn containing molecules on a surface and adjust it to a desired value. This way, we could "actively" control the degree of magnetic ordering on a surface.

The experiment is based on our recent publication [38], in which the magnetic moment of a molecular layer could be deliberately switched off and on by an externally supplied chemical stimulus. The stimulus used in this investigation is the nitrogen monoxide molecule (NO, commonly called nitric oxide). NO is a heteronuclear diatomic molecule, which can provide an uncompensated spin (S=1/2) in its π^* antibonding molecular orbital (MO). The MO diagram of NO, constructed by a linear combination of atomic orbitals (LCAO) of nitrogen (N) and oxygen (O) is shown in Figure 5.1 (a).
NO can bind with transition metals to form metal-nitrosyl complexes [4]. The bond between the metal and NO is either linear (180°), or bent ($\approx$ 120°), see Figure 5.1 (c). In the first case NO is formally considered as a three-electron-donor, in the second it supplies one electron [99]. NO has the ability of reductive nitrosylation, leading to the formation of metal-nitrosyl complexes with a lower oxidation state than the parent compound. For example, Fe(III)TPPCl was reported to react with NO in a toluene solution to give Fe(II)TPP-NO [100].

It has been demonstrated for a Co-porphyrin adsorbed on silver [101] and on nickel surface [38] that NO can selectively bind to the central metal ion of the molecule and form a metal-nitrosyl complex. Upon this reaction, presented in Figure 5.1 (b), the uncompensated spin provided by the NO paired up with one unpaired electron from the $3d_{z^2}$ orbital of the Co. Pairing of the electrons was reversible and the initial electron configuration could be restored upon thermal treatment followed by the dissociation of NO.

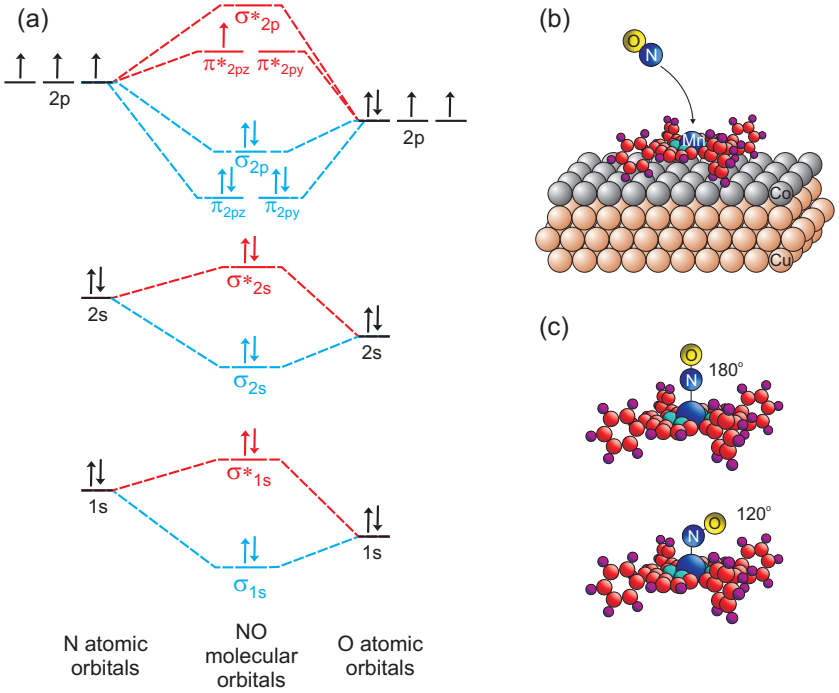

Figure 5.1: MO diagram of the NO molecule and the design of the switching experiment. (a) The blue and red orbitals are the bonding and antibonding levels, respectively. The atomic orbitals of O lie lower in energy than the corresponding orbitals of N, because they are more electronegative (after [102]). **(b)** Selective adsorption of NO at the Mn ion of the porphyrin and formation of the nitrosyl complex at the surface. **(c)** the metal-NO angle can be either linear or bent, depending on the number of electrons constituting the bond (see text).

The experiment presented here was performed on 1 ML MnTPPCl/Co(001) sample prepared by the standard procedure (see Chapter 2 for details). The molecular film was subsequently exposed to 6000 L (p= $8.25 \cdot 10^{-6}$ mbar for 1000 s) NO gas at room temperature and the consequence of this reaction was monitored by recording the Mn and Co XMCD signals.

5.1 Experiment

Mn-porphyrin on adsorbed Co(001) has been shown in previous chapters to lose the axial Cl ligand and to have three unpaired electrons in the Mn 3d orbitals leading to

$S_{Mn} = 3/2$. The magnetic moment initially present at Mn atom was manifested by the characteristic Mn XMCD signal, which was parallel to the magnetization of the substrate (Figure 5.2 (a) and (b) black curves for Mn and Co, respectively). After exposure to the NO gas, the dichroic spectrum of Mn almost completely disappeared and additionally, a small antiferromagnetic contribution has emerged. Red curve in Figure 5.2 (a) displays this change. The vanishing Mn-XMCD signal suggests that the NO acts here as a three-electron-donor compensating the spin of S=3/2 on the Mn ion, i.e. switching the molecular magnetization off. In the MnTPPCl/Co(001) system, we have shown previously that the majority of the porphyrin molecules dissociates after adsorption on Co(001) causing the loss of Cl and the subsequent reduction of the Mn oxidation state from 3+ to 2+. Part of the molecules that did not dissociate does not provide a position in the octahedral symmetry of the central metal ion, so the NO ligand cannot be accepted. These porphyrins remain magnetically coupled to the substrate.

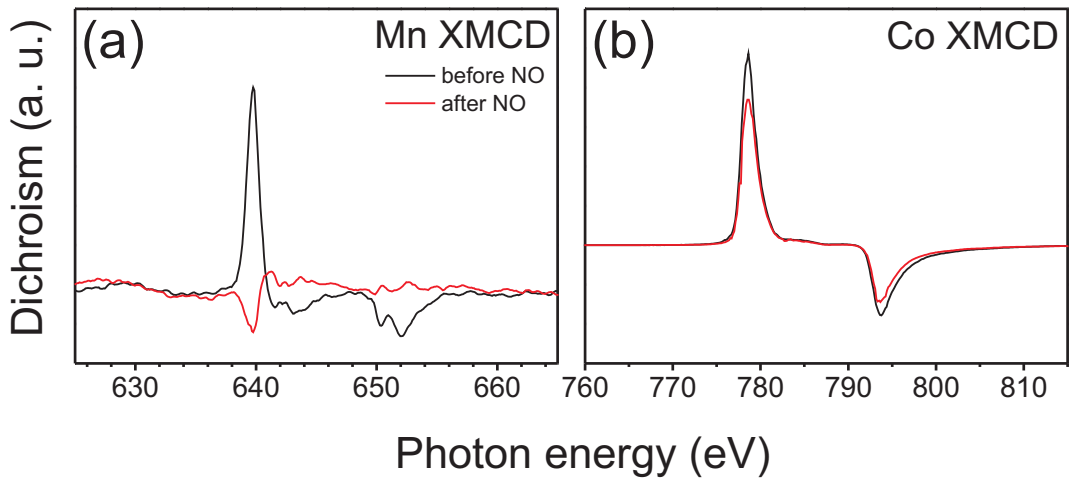

Figure 5.2: XMCD spectra of Mn and Co before and after reaction with NO. (a) The Mn XMCD signal (black) has almost disappeared after binding with NO (red). **(b)** Substrate magnetization remains nearly intact before (black) and after (red) the reaction.

One possibility of the antiferromagnetic contribution appearing in Figure 5.2 (a) is a partial oxidation of the substrate due to the reaction with NO, as it was shown in the case of the Ni(001) substrate [103]. The oxygen then acts as a mediator in the antiferromagnetic superexchange interaction between an intact MnTPPCl molecule and Co, as shown in Chapter 4 and in [37]. DFT+U calculations, which could explain the details of the magnetization reversal of Mn upon the nitrosylation are underway. It is also important to note, that the switching-off event is not related to an NO-induced modification in the substrate-molecular interaction, but is rather an effect aimed directly at the Mn ion. The magnetization of the substrate is only marginally affected by the reaction with NO, as can be clearly seen from the Co XMCD spectrum in Figure 5.2 (b). Additionally, it has been reported that in solution the nitrosylation reaction of Mn(III)TPPCl has not

been observed [104]. Therefore the here reported nitrosylation provides more evidence for the Cl dissociation as it occurs upon adsorption of the MnTPPCl molecule on the Co(001) substrate.

The X-ray absorption spectrum of Mn before and after the reaction is presented in Figure 5.3. The oxidation state of Mn is 2+ and it remains like this also upon reaction with NO. This result is in agreement with the existing literature [104]. As a consequence, we observe here a sort of reductive nitrosylation in which the initial molecule – Mn(III)TPPCl evaporated on the Co substrate reacts with NO to form Mn(II)TPP-NO compound. The substrate therefore acts as an acceptor, like in the reductive nitrosylation of Fe(III)TPPCl in a solution [105]. The XA spectrum in Figure 5.3 shows additionally a change in its spectral shape, which is an indication of the NO reacting with Mn and the subsequent change of its electronic configuration.

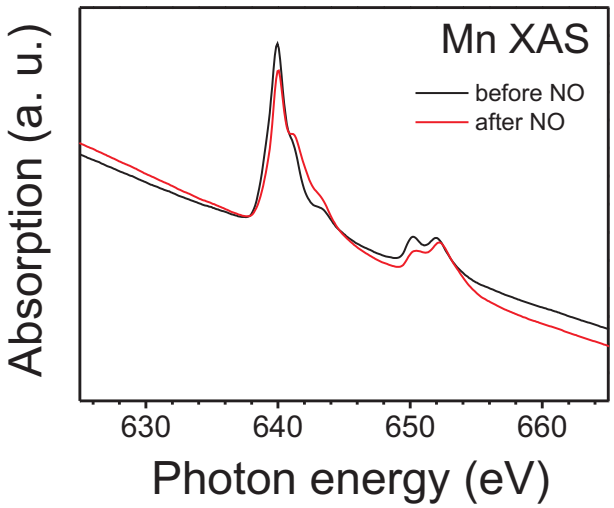

Figure 5.3: NO binding to the MnTPP molecule. XAS of Mn before and after the adsorption of NO displaying a change in the spectral shape, but not in the oxidation state.

5.2 Discussion and conclusions

To explain the observed effects of the Mn-NO bond formation and the subsequent quenching of the Mn magnetic moment, we have to characterize the geometry the newly formed bond. The critical value n defining this geometry is the number of metal d electrons plus the electron in the π^* orbital of NO. In the square pyramidal geometry of metalloporphyrins, if n=6 (five electrons in Mn3d plus one in NO) the Mn-NO bond is linear; if n=8 (e.g. in CoTPP-NO) – bent (see Figure 5.1 (c)) [105]. This formalism stems from the electron occupancy of the molecular orbitals of the MTPP-NO (M – transition metal) molecule. For n=0-6 electrons, the valence electrons occupy only the

bonding and non-bonding MOs, leaving the anti-bonding orbitals empty. This results in a maximal overlap between M and NO orbitals, leading to a linear bond.

In the linear configuration NO is formally considered as a three electron donor [99], therefore it can fully compensate the three unpaired electrons in Mn and induce the complete quenching of the Mn spin. The MO diagram for MnTPP-NO appears in Figure 5.4 (a). This diagram focuses on the metal d (left) and NO π^* (right) levels. It is important to note, that the energy level alignment for Mn(II)TPP is different than for Mn(III)TPPCl shown in Chapter 2. Here, the d_{xy} level lies below the d_π ($=d_{xz} + d_{yz}$) orbitals, due to the fact, that Mn moves out of the porphyrin plane in the Mn(II)TPP complex [106]. *It has been shown recently by DFT calculations* for Mn-phthalocyanine, that the Mn electronic states near the Fermi energy are mostly defined by the d_π orbitals, leading to a significant hybridization of d_π and NO π^* levels upon nitrosylation [107]. Therefore, the MO diagram in Figure 5.4 (a) displays the bonding between NO π^* and the degenerate Mn d_π orbitals, where the π^* electron (green) pairs up with one of the d_π electrons. The lowest possible and energetically most favourable position for the Mn d_{z^2} electron is at the bonding d_π π^* orbital (displayed in a red dashed circle in Figure 5.4 (a)). This way, all electrons in the system can be paired and no net magnetic moment is present anymore within the MnTPP-NO complex.

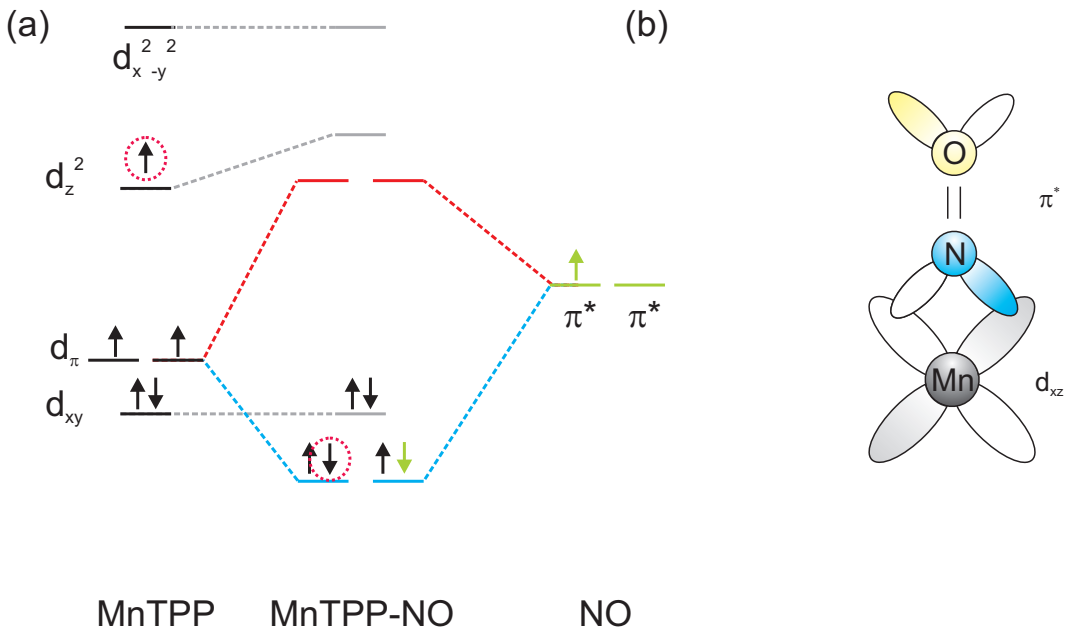

Figure 5.4: Bonding between MnTPP and NO. (a) MO diagram of the MnTPP-NO complex constructed as a LCAO of Mn 3d and NO π^* orbitals. Blue, red and gray levels denote bonding, antibonding and non-bonding orbitals, respectively (adapted from [106] and [108]). **(b)** Geometry of the π Mn-NO bond.

Furthermore, the antibonding orbitals are not occupied allowing for the maximum over-

lap between the Mn d_π and NO π^* orbitals. Therefore, NO is bound to MnTPP in linear geometry (see Figure 5.4 (b)). Notably, this geometry of the Mn-NO bond also allows for a backbonding event [99], resulting in a very strong bond between Mn and NO. Therefore, we were not able to dissociate NO from the MnTPP-NO complex by thermal treatment and restore the magnetic moment of Mn, as it was possible in case of CoTPP-NO in its bent geometry [38]. It has been shown though, that the dissociation of NO from the MnTPP-NO complex in solution can be accomplished by a 355 nm (UV) laser pulse [104].

The above described hypothesis of the Mn-NO bonding is based on our experimental observations and their correlation with the available literature. Further theoretical calculations, aimed at a more detailed understanding of the physico-chemical mechanisms involved in the switching event are underway.

CHAPTER 6

Summary and outlook

This thesis provides a detailed study of the magnetic properties of manganese tetraphenylporphyrin chloride (MnTPPCl) adsorbed onto ferromagnetic cobalt (Co) thin films. MnTPPCl on Co served as the model system for identifying the relevant factors influencing the magnetic coupling of this organic adsorbate to the magnetic substrate. Generally, a prerequisite to the magnetization is the occurrence of unpaired electrons in the system. The number of unpaired electrons defines the total spin of the system containing electrons, like a molecule or atom. At close proximity, neighbouring spin systems interact via the exchange interaction, and for a large-enough number of closely interacting spin systems, e.g. in bulk iron, the orientation is correlated within the so-called ferromagnetic domains. The spins interact with an external magnetic field such that their reorientation may occur starting from domain boundaries. In the special case of a molecular monolayer composed of porphyrins, the lateral distance between the spins is too large; consequently the lateral coupling is insufficient for this layer to be naturally ferromagnetic. However, by putting a paramagnetic molecule in close vicinity to a ferromagnetic substrate, one can "pin" the molecular spin on a surface by molecule-substrate magnetic coupling. This behaviour has been accessed with the element-specific X-ray magnetic circular dichroism technique. By systematic modification of the electronic structure of the magnetic centre of the molecule, or by interaction of its bonding with the substrate, further insight has been provided during the progress of this thesis. The thorough understanding of all chemical, electronic and thermodynamic processes that can occur on a surface is a prerequisite to understand the behaviour of magnetic molecules at surfaces. Importantly, surface supported magnetic molecules not only provide model interfaces for studies about processes which also occur within the device

active interfaces in spintronic devices, but also open-up the possibility to modify and probe spin by an externally supplied stimulus, e.g. with scanning probe instruments.

The initial goal of the research was to investigate the nature of the magnetic coupling between the Mn-porphyrin and the magnetic Co substrate. In view of this objective we have compared the magnitudes of the Mn magnetic dichroism signal (XMCD) for the molecules adsorbed on smooth and on rough Co films and thereby provided an experimental proof towards an indirect exchange interaction between the Mn and the Co. Density functional theory (DFT and DFT+U) calculations performed for the system under study confirmed the indirect exchange mechanism and additionally showed that the coupling occurred through nitrogen atoms of the porphyrin ring. The calculations also predicted that the non-planar molecule with an axially coordinated Cl-ligand can only adsorb in the Cl-up geometry, i.e. with Cl oriented away from the substrate. In the case of Cl-down adsorption, theory predicted breaking of the Mn-Cl bond and a subsequent adsorption of a reduced Mn(II)TPP species on the substrate. Therefore, both species: Mn(II)TPP and Mn(III)TPPCl are expected to coexist on the Co surface.

In the course of the project we have also discovered that oxidation of the ferromagnetic Co surface can substantially change not only the properties of the substrate itself but also the type of its interaction with the Mn-porphyrin. By scanning tunneling microscopy (STM) we have studied the molecular distribution on both substrates and have observed the molecular self-assembly on the O/Co, which was not occurring on Co. This fact implies that the interaction by directional, possibly "chemical" bonds of the O/Co was lowered compared to the atomically clean Co. The most striking difference caused by the oxidation of the Co was the change of the molecule-substrate magnetic interaction. The initial ferromagnetic indirect exchange interaction turned into an antiferromagnetic superexchange coupling leading to an opposite alignment of the Mn and the Co spins. Additionally, by means of X-ray absorption spectroscopy (XAS) we have found that the oxidation state of the Mn species adsorbed on the atomically clean Co was predominantly reduced from 3+ to 2+. Such reduction indicates a removal of the axially coordinated Cl-ligand, which was previously predicted by the DFT calculations (see above). On the oxygen reconstructed Co the Mn X-ray absorption spectra manifested the existence of a 3+ Mn species i.e. the intact Mn(III)TPPCl molecule. This observation of the stability of Mn(III)TPPCl upon adsorption on O/Co is in good agreement with the assignment of a lower chemical reactivity of the oxygen-reconstructed Co substrate, as previously mentioned.

The removal of Cl upon adsorption of MnTPPCl on Co was eventually confirmed by performing a surface supported chemical reaction with nitric oxide (NO). The empty position in the octahedral symmetry of the Mn atom left after Cl dissociation could be used as a grip for a newly supplied NO ligand. The reaction with NO has been a successful attempt of manipulation of the molecular spin on the surface and also confirmed

the Mn spin configuration on Co derived from the previous experiment. Mn species adsorbed on Co was shown in Chapter 4 to exist in an intermediate spin configuration with $S_{Mn} = 3/2$, i.e. with three unpaired electrons in the Mn 3d orbitals. Attachment of NO, caused reorganization of the spins allowing for a consequent switching off of the molecular magnetization. At the same time, the magnetization of the substrate remained nearly unchanged. Due to a particular bonding situation, the dissociation of NO from the MnTPP-NO species by thermal treatment was not possible and the molecular magnetization remained switched-off. Despite the irreversibility of the reaction, the experiment showed that an organic spintronic device is no longer a fiction, but a real, feasible to achieve aim of the molecular surface science.

Our study of Mn-porphyrin adsorbed on Co substrates not only revealed remarkable properties of the system, but also demonstrated the strength of the spectro-microscopy correlation approach to study the magnetism and the structure of organometallic interfaces. This approach, here involving XMCD, XAS, and STM raised new issues important for the determination of molecular adsorption scheme as well as for the physical/chemical bonding and, consequent electronic structure of the molecules. Finally, combination of the experiment with theoretical models uniquely highlighted the interplay of molecular geometry and chemical and magnetic interactions in an unprecedented way.

The paragraphs above summarize the major phenomena discovered experimentally and theoretically during this research project. Still the exact molecule-substrate interaction poses many open questions. From the molecular assembly in the STM images it is evident that the molecule-substrate interaction is stronger on Co than on O/Co. Additionally, the Cl-dissociation from the molecules adsorbed on Co further confirms a substantial influence of the surface on the porphyrin. Strong interaction would imply a chemisorption and therefore creation of a bond between the molecule and the substrate, which consequently should lead to a direct magnetic exchange interaction. Neither the chemisorption nor the direct exchange have been confirmed by theoretical calculations. Similarly, on O/Co the molecular self-assembly observed in the STM images suggests a weak interaction with the surface (i.e. physisorption), which explains the observation that the molecular integrity stays intact upon adsorption on this substrate. "Physisorption" suggests an interaction without a directional chemical bond between Mn and O, which, again, contradicts the calculations. We should, though, keep in mind that a clear distinction between chemi- and physisorption fails for complex π-conjugated organic molecules [109]. Therefore one should not make assumptions about substrate-molecule interactions based on the computed distances. Both types of adsorption could, in principle, lead to a stronger or weaker interaction and the type of magnetic exchange coupling would then only depend on the, e.g. adsorption site, geometry of interacting orbitals and their electron occupancy. Towards the assessment of the here raised issues a large volume of additional experimental work has to be performed. We believe that resolving

these questions would lead to a more precise understanding and prediction of the magnetic properties of organic monolayers. This would allow for the design of spintronic devices with desirable properties and tunable magnetization.

Future investigations of the molecular surface magnetism will include modification of various determinants of the system. Different transition metals in the centre of the molecule would create a new electron configuration and therefore – spin. For example, for Co(III)TPPCl the total number of 3d electrons equals 6, which, depending on their distribution over the orbitals, could yield a spin of either $S_{Co} = 2$ (high-spin, HS), or $S_{Co} = 0$ (low-spin, LS) or some intermediate-spin (IS) value. If the Cl dissociation also occurred for this molecule, then the number of 3d electrons would increase to 7 and the respective spin configurations would amount: $S_{Co} = 3/2$ (HS) and $S_{Co} = 1/2$ (LS). Probing such a system with XMCD[1], XAS[1] and STM on atomically clean and oxygen modified substrates could yield information about the universality of our experimental observations and bring new insights into the discussed Cl-issue.

Another issue affecting the magnetic behaviour of molecules is the distance to the substrate. It can be modified by varying the type of the molecule. Mn-phthalocyanine (MnPcCl), for example, should adsorb closer to the Co substrate, as it does not contain flexible phenyl rings present in the MnTPPCl. It has been mentioned in the Introduction (Chapter 1) that various phthalocyanine molecules undergo a charge transfer reaction with the substrate, leading to a new electron configuration. It might also become possible to observe a direct magnetic exchange interaction between the molecular centre and the surface, if the distance between the two atoms was sufficiently low.

The influence of the substrate symmetry might also have an impact on the magnetic properties of the molecules. Depending on the adsorption site (hollow versus bridge, or on-top) the interaction with the substrate could probably change due to the possibility of different orbital contributions to the coupling mechanism. It would be therefore desirable to determine the preferred adsorption site of molecules adsorbed on a (001) fcc surface and compare it with, for example, the (111) fcc plane. The knowledge gained by such an experiment might lead, in the future, to a design of organic spintronic interfaces with suitable, well controlled properties.

The molecular magnetization on the surface could be adjusted by the use of different chemical compounds as stimuli. There have been examples (see Chapter 1) of carbon monoxide (CO) or ammonia (NH_3) used as externally supplied ligands to an Fe-phthalocyanine (FePc) molecule. Both molecules were shown to quench the magnetization of the FePc. Different ligand-magnetic molecule combinations should make it possible to tune the spin state of the molecular magnetic centre to a desired value.

[1] In the case of CoTPPCl adsorption it is also essential to change the substrate from Co to some other ferromagnetic metal, for example Ni. Otherwise, the distinction between the molecular and the substrate cobalt species would not be possible by means of XMCD or XAS.

A promising candidate for the purpose of magnetic switching (as a ligand) is also an organic molecule: tetracyano-p-quinodimethane (TCNQ). It is a strong electrophile and could therefore induce a charge tranfer from the central metal of the poprhyrin, leading to modification of the Mn spin-state. An attractive modification of the switching experiment would be the use, instead of a chemical stimulus, a physical one, for example a laser pulse. Light-induced switching of the molecule's magnetization on a surface would have a high impact on future applications, as it would prevent dosing toxic gases to a potential device. A tempting follow-up experiment of the switching event is a simultaneous switching-on and -off of a two-molecule-mixed-layer using the same (physical or chemical) stimulus. This way, a controlled selective switching within a complex surface layer could be achieved. Such experiments, in conjunction with a designed hydrogen-bonded supramolecular surface network would constitute a "magnetic checkerboard" where the magnetization of neighbouring fields could be flipped.

Bibliography

[1] J. Ellis, *Forbidden Rites: Your Complete Guide to Traditional Witchcraft*, O Books, 1st edition, 2009.

[2] A. Fert, *Reviews of Modern Physics* **80**, 1517 (2008).

[3] V. A. Dediu, L. E. Hueso, I. Bergenti, and C. Taliani, *Nature Materials* **8**, 707 (2009).

[4] J. E. Huheey, E. A. Keiter, and R. L. Keiter, *Inorganic Chemistry: principles of structure and reactivity*, Prentice Hall, 4th edition, 1997.

[5] M. N. Baibich, J. M. Broto, A. Fert, F. N. van Dau, F. Petroff, P. Etienne, G. Creuzet, A. Friederich, and J. Chazelas, *Physical Review Letters* **61**, 2472 (2007).

[6] G. Binasch, P. Grünberg, and W. Zinn, *Physical Review B* **39**, 4828 (1989).

[7] S. Sanvito, *Nature Materials* **6**, 803 (2007).

[8] W. J. M. Naber, S. Faez, and W. G. van der Wiel, *Journal of Physics D-Applied Physics* **40**, R205 (2007).

[9] M. Mannini, F. Pineider, P. Sainctavit, L. Joly, A. Fraile-Rodriguez, M. A. Arrio, C. C. D. Moulin, W. Wernsdorfer, A. Cornia, D. Gatteschi, and R. Sessoli, *Advanced Materials* **21**, 167 (2009).

[10] J. R. Friedman, M. P. Sarachik, J. Tejada, and R. Ziolo, *Physical Review Letters* **76**, 3830 (1996).

[11] L. Bogani, L. Cavigli, M. Gurioli, R. L. Novak, M. Mannini, A. Caneschi, F. Pineider, R. Sessoli, M. Clemente-Leon, E. Coronado, A. Cornia, and D. Gatteschi, *Advanced Materials* **19**, 3906 (2007).

[12] N. Grumbach, A. Barla, L. Joly, B. Donnio, G. Rogez, E. Terazzi, J.-P. Kappler, and J.-L. Gallani, *The European Physical Journal B* **73**, 103 (2010).

[13] M. Mannini, F. Pineider, P. Sainctavit, C. Danieli, E. Otero, C. Sciancalepore, A. M. Talarico, M. A. Arrio, A. Cornia, D. Gatteschi, and R. Sessoli, *Nature Materials* **8**, 194 (2009).

[14] A. Scheybal, T. Ramsvik, R. Bertschinger, M. Putero, F. Nolting, and T. A. Jung, *Chemical Physics Letters* **411**, 214 (2005).

[15] H. Wende, M. Bernien, J. Luo, C. Sorg, N. Ponpandian, J. Kurde, J. Miguel, M. Piantek, X. Xu, P. Eckhold, W. Kuch, K. Baberschke, P. M. Panchmatia, B. Sanyal, P. M. Oppeneer, and O. Eriksson, *Nature Materials* **6**, 516 (2007).

[16] C. Iacovita, M. V. Rastei, B. W. Heinrich, T. Brumme, J. Kortus, L. Limot, and J. P. Bucher, *Physical Review Letters* **101**, 116602 (2008).

[17] S. A. Wolf, D. D. Awschalom, R. A. Buhrman, J. M. Daughton, S. von Molnar, M. L. Roukes, A. Y. Chtchelkanova, and D. M. Treger, *Science* **294**, 1488 (2001).

[18] I. Zutic, J. Fabian, and S. Das Sarma, *Reviews of Modern Physics* **76**, 323 (2004).

[19] Z. H. Xiong, D. Wu, Z. Valy Vardeny, and J. Shi, *Nature* **427**, 821 (2004).

[20] C. Joachim, J. K. Gimzewski, and A. Aviram, *Nature* **408**, 541 (2000).

[21] C. Chappert, A. Fert, and F. N. van Dau, *Nature Materials* **6**, 813 (2007).

[22] S. Javaid, M. Bowen, S. Boukari, L. Joly, J.-B. Beaufrand, X. Chen, Y. J. Dappe, F. Scheurer, J.-P. Kappler, J. Arabski, W. Wulfhekel, M. Alouani, and E. Beaurepaire, *Physical Review Letters* **105**, 077201 (2010).

[23] M. Bernien, J. Miguel, C. Weis, M. E. Ali, J. Kurde, B. Krumme, P. M. Panchmatia, B. Sanyal, M. Piantek, P. Srivastava, K. Baberschke, P. M. Oppeneer, O. Eriksson, W. Kuch, and H. Wende, *Physical Review Letters* **102**, 047202 (2009).

[24] J. Brede, N. Atodiresei, S. Kuck, P. Lazic, V. Caciuc, Y. Morikawa, G. Hoffmann, S. Blügel, and R. Wiesendanger, *Physical Review Letters* **105**, 047204 (2010).

[25] N. Tsukahara, K. Noto, M. Ohara, S. Shiraki, N. Takagi, Y. Takata, J. Miyawaki, M. Taguchi, A. Chainani, S. Shin, and M. Kawai, *Physical Review Letters* **102**, 167203 (2009).

[26] C. Isvoranu, B. Wang, K. Schulte, E. Ataman, J. Knudsen, J. N. Andersen, M. L. Bocquet, and J. Schnadt, *Journal of Physics: Condensed Matter* **22**, 472002 (2010).

[27] P. Gargiani, M. Angelucci, C. Mariani, and M. G. Betti, *Physical Review B* **81**, 085412 (2010).

[28] Z. Li, B. Li, J. Yang, and J. G. Hou, *Accounts of Chemical Research* **43**, 954 (2010).

[29] S. Narioka, H. Ishii, D. Yoshimura, M. Sei, Y. Ouchi, K. Seki, S. Hasegawa, T. Miyazaki, Y. Harima, and K. Yamashita, *Applied Physics Letters* **67**, 1899 (1995).

[30] A. Scarfato, S.-H. Chang, S. Kuck, J. Brede, G. Hoffmann, and R. Wiesendanger, *Surface Science* **602**, 677 (2008).

[31] M. Abel, S. Clair, O. Ourdjini, M. Mossoyan, and L. Porte, *Journal of American Chemical Society* **133**, 1203 (2011).

[32] L. Ramoino, M. von Arx, S. Schintke, A. Baratoff, H.-J. Güntherodt, and T. A. Jung, *Chemical Physics Letters* **417**, 22 (2006).

[33] S. Maier, L.-A. Fendt, L. Zimmerli, T. Glatzel, O. Pfeiffer, F. Diederich, and E. Meyer, *Small* **4**, 1115 (2008).

[34] W. Auwärter, A. Weber-Bargioni, A. Riemann, A. Schiffrin, O. Gröning, R. Fasel, and J. V. Barth, *The Journal of Chemical Physics* **124**, 194708 (2006).

[35] M. Casarin, M. Di Marino, D. Forrer, M. Sambi, F. Sedona, E. Tondello, A. Vittadini, V. Barone, and M. Pavone, *Journal of Physical Chemistry C* **114**, 2144 (2010).

[36] M. Koudia, M. Abel, C. Maurel, A. Bliek, D. Catalin, M. Mossoyan, J.-C. Mossoyan, and L. Porte, *Journal of Physical Chemistry B* **110**, 10058 (2006).

[37] D. Chylarecka, C. Wäckerlin, T. K. Kim, K. Müller, F. Nolting, A. Kleibert, N. Ballav, and T. A. Jung, *Journal of Physical Chemistry Letters* **1**, 1408 (2010).

[38] C. Wäckerlin, D. Chylarecka, A. Kleibert, K. Müller, C. Iacovita, F. Nolting, T. A. Jung, and N. Ballav, *Nature Communications* **1:61** (2010).

[39] K. Nilson, J. Ahlund, B. Brena, E. Göthelid, J. Schiessling, N. Martensson, and C. Puglia, *The Journal of Chemical Physics* **127**, 114702 (2007).

[40] H. Spillmann, A. Kiebele, M. Stöhr, T. A. Jung, D. Bonifazi, F. Cheng, and F. Diederich, *Advanced Materials* **18**, 275 (2006).

[41] N. Wintjes, D. Bonifazi, F. Cheng, A. Kiebele, M. Stöhr, T. A. Jung, H. Spillmann, and F. Diederich, *Angewandte Chemie* **119**, 4167 (2007).

[42] D. Ecija, K. Seufert, D. Heim, W. Auwärter, C. Aurisicchio, C. Fabbro, D. Bonifazi, and J. V. Barth, *ACS Nano* **4**, 4936 (2010).

[43] J. Lobo-Checa, M. Matena, K. Müller, J. H. Dil, F. Meier, L. H. Gade, T. A. Jung, and M. Stöhr, *Science* **325**, 300 (2009).

[44] L. G. Teugels, L. G. Avila-Bront, and S. J. Sibener, *Journal of Physical Chemistry C* **115**, 2826 (2011).

[45] A. Mugarza, N. Lorente, C. Ordejon, C. Krull, S. Stepanow, M.-L. Bocquet, J. Fraxedas, G. Ceballos, and P. Gambardella, *Physical Review Letters* **105**, 115702 (2010).

[46] R. Raval, *Chemical Society Reviews* **38**, 707 (2009).

[47] M. Takada and H. Tada, *Chemical Physics Letters* **392**, 265 (2004).

[48] G. E. Collins, K. W. Nebesny, C. D. England, L.-K. Chau, P. A. Lee, B. A. Parkinson, and N. R. Armstrong, *Journal of Vacuum Science & Technology A* **10**, 2902 (1992).

[49] J. C. Vickerman and I. S. Gilmore, *Surface Analysis the Principal Techniques*, John Wiley & Sons Ltd., 2009.

[50] K. Oura, V. G. Lifshits, A. A. Saranin, A. V. Zotov, and M. Katayama, *Surface Science an Introduction*, Springer-Verlag, 2003.

[51] C. Sorg, N. Ponpandian, M. Bernien, K. Baberschke, H. Wende, and R. Q. Wu, *Physical Review B* **73**, 064409 (2006).

[52] J. F. Moulder, W. F. Stickle, P. E. Sobol, and K. D. Bomben, *Handbook of X-ray Photoelectron Spectroscopy*, Perkin-Elmer Corporation, 1992.

[53] C. J. Chen, *Introduction to Scanning Tunneling Mircroscopy*, Monographs on the Physics and Chemistry of Materials, Oxford Univerity Press Inc., 2008.

[54] R. Wiesendanger, H.-J. Güntherodt, G. Güntherodt, R. J. Gambino, and R. Ruf, *Physical Review Letters* **65**, 247 (1990).

[55] R. Wiesendanger, H. J. Guntherodt, G. Guntherodt, R. J. Gambino, and R. Ruf, *Physical Review Letters* **65**, 247 (1990).

[56] *X-ray Data Booklet*, Lawrence Berkeley National Laboratory, 2009.

[57] http://www.lightsources.org/cms/?pid=1000098.

[58] J. Stöhr and H. C. Siegmann, *Magnetism: from Fundamentals to Nanoscale Dynamics*, volume 152 of *Springer Series in Solid-State Sciences*, Springer Verlag, Berlin, 2006.

[59] D. M. Mills, J. R. Helliwell, A. Kvick, T. Ohta, I. A. Robinson, and A. Authier, *Journal of Synchrotron Radiation* **12**, 385 (2005).

[60] D. Jiles, *Introduction to Magnetism and Magnetic Materials*, Taylor & Francis Group, 1998.

[61] E. Beaurepaire, H. Bulou, F. Scheurer, and J.-P. Kappler, *Magnetism: a Synchrotron Radiation Approach*, Lecture Notes in Physics, Springer-Verlag, 2006.

[62] U. Fano, *Physical Review Letters* **124**, 1866 (1961).

[63] B. T. Thole, P. Carra, F. Sette, and G. Vanderlaan, *Physical Review Letters* **68**, 1943 (1992).

[64] P. Carra, B. T. Thole, M. Altarelli, and X. D. Wang, *Physical Review Letters* **70**, 694 (1993).

[65] C. T. Chen, Y. U. Idzerda, H. J. Lin, N. V. Smith, G. Meigs, E. Chaban, G. H. Ho, E. Pellegrin, and F. Sette, *Physical Review Letters* **75**, 152 (1995).

[66] C. Piamonteze, P. Miedema, and F. M. F. de Groot, *Physical Review B* **80**, 184410 (2009).

[67] U. Flechsig, F. Nolting, A. F. Rodriguez, J. Krempasky, C. Quitmann, T. Schmidt, S. Spielmann, and D. Zimoch, *AIP Conference Proceedings* **1234**, 319 (2010).

[68] L. R. Milgrom, *The Colours of Life*, Oxford University Press, 1997.

[69] S. Berner, M. de Wild, L. Ramoino, S. Ivan, A. Baratoff, H.-J. Güntherodt, H. Suzuki, D. Schlettwein, and T. A. Jung, *Physical Review B* **68**, 115410 (2003).

[70] T. A. Jung, R. R. Schlittler, and J. K. Gimzewski, *Nature* **386**, 696 (1997).

[71] D. V. Behere and S. Mitra, *Inorganic Chemistry* **19**, 992 (1980).

[72] H. P. Oepen, M. Benning, H. Ibach, C. M. Schneider, and J. Kirchner, *Journal of Magnetism and Magnetic Materials* **86**, L137 (1990).

[73] M. Treier, P. Ruffieux, R. Schillinger, T. Greber, K. Müllen, and R. Fasel, *Surface Science* **602**, L84 (2008).

[74] T. A. Jung, R. R. Schlittler, J. K. Gimzewski, H. Tang, and C. Joachim, *Science* **271**, 181 (1996).

[75] J. Stöhr, *NEXAFS Spectroscopy*, Springer, 1st edition, 1992.

[76] S. Kuck, M. Prostak, M. Funk, M. Bröring, G. Hoffman, and R. Wiesendanger, *Journal of Vacuum Science and Technology A* **28**, 795 (2010).

[77] P. J. Thomassen, *Cooperative porphyrin assemblies*, PhD thesis, Radboud Universiteit, 2006.

[78] W. R. Scheidt and C. A. Reed, *Chemical Reviews* **81**, 543 (1981).

[79] M. E. Ali, B. Sanyal, and P. M. Oppeneer, *Journal of Physical Chemistry C* **113**, 14381 (2009).

[80] P. M. Oppeneer, P. M. Panchmatia, B. Sanyal, O. Eriksson, and M. E. Ali, *Progress in Surface Science* **84**, 18 (2009).

[81] D. Chylarecka, T. Kim, K. Tarafder, K. Müller, K. Gödel, I. Czekaj, C. Wäckerlin, M. Cinchetti, M. E. Ali, C. Piamonteze, F. Schmitt, W. J.-P., C. Ziegler, F. Nolting, M. Aeschlimann, P. Oppeneer, N. Ballav, and T. Jung, *Journal of Physical Chemistry C* **115**, 1295 (2011).

[82] C. E. Housecroft and A. G. Sharp, *Inorganic Chemistry*, New York, 3rd ed. edition, 2008.

[83] S. Konishi, M. Hoshino, and M. Imamura, *Journal of Physical Chemistry* **86**, 1412 (1982).

[84] B. Gonzalez, J. Kouba, S. Yee, C. A. Reed, J. F. Kirner, and W. R. Scheidt, *Journal of the American Chemical Society* **97**, 3247 (1975).

[85] M.-S. Liao, J. D. Watts, and M.-J. Huang, *Inorganic Chemistry* **44**, 1941 (2005).

[86] H.-J. Freund, H. Kuhlenbeck, and V. Staemmler, *Reports on Progress in Physics* **59**, 283 (1996).

[87] Z. Y. Yang and C. Durkan, *Surface Science* **604**, 660 (2010).

[88] J. V. Barth, *Annual Review of Physical Chemistry* **58**, 375 (2007).

[89] J. M. Gottfried and H. Marbach, *Zeitschrift Fur Physikalische Chemie-International Journal of Research in Physical Chemistry & Chemical Physics* **223**, 53 (2009).

[90] C. M. Drain, A. Varotto, and I. Radivojevic, *Chemical Reviews* **109**, 1630 (2009).

[91] F. Schreiber, *Progress in Surface Science* **65**, 151 (2000).

[92] D. E. Barlow, L. Scudiero, and K. W. Hipps, *Langmuir* **20**, 4413 (2004).

[93] H. Yanagi, K. Ikuta, H. Mukai, and T. Shibutani, *Nano Letters* **2**, 951 (2002).

[94] S. Berner, M. Brunner, L. Ramoino, H. Suzuki, H. J. Guntherodt, and T. A. Jung, *Chemical Physics Letters* **348**, 175 (2001).

[95] X. Bai, X. Hu, S. Zhou, J. Yan, C. Sun, P. Chena, and L. Laifeng, *Journal of Materials Chemistry* **21**, 7123 (2011).

[96] K. Doll and N. M. Harrison, *Physical Review B* **63**, 165410 (2001).

[97] K. Kishi and S. Ikeda, *The Journal of Physical Chemistry* **78**, 107 (1974).

[98] A. G. Wren, R. W. Phillips, and L. U. Tolentino, *Journal of Colloid and Interface Science* **70**, 544 (1979).

[99] L. J. Ignarro, *Nitric oxide: biology and pathobiology*, Academic Press, 1st edition, 2000.

[100] P. C. Ford and I. M. Lorkovic, *Chemical reviews* **102**, 993 (2002).

[101] K. Flechtner, A. Kretschmann, H.-P. Steinrück, and J. M. Gottfried, *Journal of the American Chemical Society* **129**, 12110 (2007).

[102] J. A. McCleverty, *Chemical Reviews* **104**, 403 (2004).

[103] A. Sandell, A. Nilsson, and N. Martensson, *Surface science* **251-252**, 971 (1991).

[104] H. Adachi, H. Sonoki, M. Hoshino, M. Wakasa, H. Hayashi, and Y. Miyazaki, *Journal of physical chemistry A* **105**, 392 (2001).

[105] W. R. Scheidt and M. K. Ellison, *Accounts of Chemical Research* **32**, 350 (1999).

[106] L. J. Boucher, *Journal of the American Chemical Society* **92**, 2725 (1970).

[107] T. Q. Nguyen, M. C. Escano, and H. Kasai, *Journal of Physical Chemistry B* **114**, 10017 (2010).

[108] T. W. Hawkins and M. B. Hall, *Inorganic Chemistry* **19**, 1735 (1980).

[109] A. Kara, K. Müller, T. Brugger, T. Greber, and T. A. Jung, *submitted* (2011).

Acknowledgements

This thesis is a result of my three-and-a-half year long stay at PSI. During that time, I have worked in an international group of scientists, who have taught me valuable lessons about different aspects of the project. In the paragraphs below I thank all my colleagues and coworkers in order of their appearance in my PhD life.

In the first place I thank my PSI supervisor Thomas Jung, who hired me for this project and has supported me all throughout. He has always encouraged the good spirit in our team even during nerve-wracking and often unsuccessful beamtimes. Merci.

I thank my first collaborators and office mates: Kathrin Müller and Timur Kim who introduced me into the world of surface science, experimental techniques and revealed all the secrets of the UHV to me. Danke, Спасибо.

I am grateful to our oustanding technician Rolf Schelldorfer – a Toyota enthusiast and very generous owner of the coffee machine. Without Rolf the lab would be a useless tangle of cables where no single piece of equipment works. Danke.

I would also like to thank the LMN secretary and a fabulous organiser Edith Meisel. She has been a great help in all administrative matters and has helped me solving several problems. Merci.

A very important person in my PhD life has been Ernst Meyer – my doctor-father at Basel University who accepted me as his student and stimulated interesting discussions about my project. I am grateful for his friendliness and valuable comments. Danke.

The SIM beamline staff: Frithjof Nolting, Cinthia Piamonteze (now at Xtreme), Armin Kleibert, Arantxa Fraile Rodriguez (now in Barcelona) and Andrea Steger (now at Sensirion). Thank you for your proffesional advice, sense of humour and patience even when I had to call at 3 a.m. for instructions. Danke, Obrigada, Gracias.

I am grateful to my current coworkers: Nirmalya Ballav, André Kaufmann, Christian Wäckerlin, Tatjana Hählen and Jan Girovsky. It has been a great pleasure to work with you and every day learn something new together. Special thanks are to Nirmalya – for his enthusiasm and support (even from India) and for writing papers and proposals together. Dhonnobad, Merci, D'akujem.

Apart from the professional part of my thesis, there was also a big private contribution from friends, with whom I have spent my after-work life: Ana, Stefan, Anja, Günther, Maxi (with Alessandro), Andrea, Olga, Valerio, Miryam, Dirk, Zeljka, Iza, Slawo, Darek N., Darek C., Miłosz, Marcin, Rafał, Darek J., Gosia, Janek, Agnieszka, Christian B., Raquel, Elena, and many more. Thanks for being with me. Gracias, Danke, Grazie, Спасибо, Hvala, Dziękuję.

The biggest thank you is to my family and to Piotr for their support during my education, for all the encouragement and their love. Dziękuję Wam.

Curriculum vitae

Name: **Dorota Chylarecka**
Born: 26 July 1983, Poznań, Poland
Nationality: Polish

Education:

2008–2011 PhD in surface science, University of Basel, Basel, Switzerland

2005–2007 MSc. in solid states physics, AGH University of Science and Technology, Kraków, Poland

2002–2004 BSc. Engineer in solid states physics, AGH University of Science and Technology, Kraków, Poland

Internships:

2004–2005 Socrates-Erasmus students' exchange programme, Technical University Clausthal, Clausthal-Zellerfeld, Germany

2006 Summer student at the Swiss Light Source, Paul Scherrer Institut, Villigen, Switzerland

The following professors have contributed to my education:

Thomas Jung, Ernst Meyer, Wojciech Łużny, Czesław Kapusta, Krzysztof Malarz, Józef Korecki, Andrzej Lenda, Jacek Tarasiuk, Paweł Gryboś, Rafał Kalinowski

Publication list

The following lists are compilations of scientific articles and conference contributions, which were accomplished during the course of the project.

Scientific articles:

1. D. Chylarecka, C. Wäckerlin, T. K. Kim, K. Müller, F. Nolting, A. Kleibert, N. Ballav, and T. A. Jung, "Self-assembly and superexchange coupling of magnetic molecules on oxygen-reconstructed ferromagnetic thin film" *Journal of Physical Chemistry Letters* **1**, 1408 (2010).

2. C. Wäckerlin, D. Chylarecka, A. Kleibert, K. Müller, C. Iacovita, F. Nolting, T. A. Jung, and N. Ballav, "Controlling spins in adsorbed molecules by a chemical switch" *Nature Communications* **1:61** (2010).

3. D. Chylarecka, *et al.* "Indirect magnetic coupling of manganese porphyrin to a ferromagnetic cobalt substrate" *Journal of Physical Chemistry C* **115**, 1295 (2011).

4. C. Wäckerlin, K. Tarafdar, D. Chylarecka, A. Kleibert, C. Iacovita, F. Nolting, T. A. Jung, P. M. Oppeneer and N. Ballav, "Complexity of surface spin-trans effect unveiled at quantum level" *in preparation* (2011).

5. D. Chylarecka *et al.* "Manganese-porphyrin and manganese-phthalocyanine: exchange coupling and molecular assembly on ferromagnetic substrates" *in preparation* (2011).

6. C. Wäckerlin, C. Iacovita, D. Chylarecka, P. Fesser, T. A. Jung and N. Ballav, "Assembly of 2D ionic layers by reaction of alkali halides with the organic electrophile 7,7,8,8-tetracyano-p-quinodimethane (TCNQ)" *Chemical Communications* **47**, 9146 (2011).

Conference contributions:

1. D. Chylarecka, K. Müller, C. Wäckerlin, N. Ballav, and T. A. Jung, "Research opportunities at Nanojunction Lab at Laboratory for Micro- and Nanotechnology, Paul Scherrer Institute" *Swiss-Polish Science and Technology Days*, Warsaw, Poland, January 14-15.2010

2. D. Chylarecka, C. Wäckerlin, T. K. Kim, K. Müller, F. Nolting, A. Kleibert, N. Ballav, and T. A. Jung, "Assembly and exchange coupling of magnetic molecules on metallic and oxygen reconstructed ferromagnetic thin films" *26th SAOG meeting*, Fribourg, Switzerland, January 22nd, 2010

3. D. Chylarecka, C. Wäckerlin, T. K. Kim, K. Müller, F. Nolting, A. Kleibert, N. Ballav, and T. A. Jung, "Self-assembly and superexchange coupling of magnetic molecules on metallic and oxygen reconstructed ferromagnetic thin films" *6th Progress Meeting, Marie Curie - Research Training Network (FP6) PRAIRES*, Basel, Switzerland, April 15th, 2010

4. D. Chylarecka, C. Wäckerlin, T. K. Kim, K. Müller, F. Nolting, A. Kleibert, N. Ballav, and T. A. Jung, "Exchange coupling and assembly of magnetic molecules on ferromagnetic substrates" *18th International Vacuum Congress (IVC-18)*, Beijing, China, August 23-27.2010

5. D. Chylarecka, C. Wäckerlin, T. K. Kim, K. Müller, F. Nolting, A. Kleibert, N. Ballav, and T. A. Jung, "Exchange coupling and assembly of magnetic molecules

on ferromagnetic substrates" *The 27th European Conference on Surface Science (ECOSS27)*, Groningen, Netherlands, August 28th-September 3rd 2010

6. D. Chylarecka, T. K. Kim, K. Müller, C. Wäckerlin, E. Meyer, N. Ballav, F. Nolting and T. A. Jung, "Growth and magnetic properties of metallo-porphyrins on magnetic substrates" poster at *8th PSI Summer School on Condensed Matter Research*, Zuoz, Switzerland, August 1-7.2009

7. D. Chylarecka, C. Wäckerlin, T. K. Kim, K. Müller, F. Nolting, A. Kleibert, N. Ballav and T. A. Jung, "Self-assembly and superexchange coupling of magnetic molecules on metallic and mxygen-reconstructed ferromagnetic thin films" poster at *9th Site Visit of the Review Panel NCCR Nanoscale Science*, Basel, Switzerland, April 27th, 2010